Metal-Metal Multiple Bonds in Ordered Assemblies. 1. Tetranuclear Molybdenum and Tungsten Carboxylates Involving Covalently Linked M-M Quadruple Bonds. Molecular Models for Subunits of One-Dimensional Stiff-Chain Polymers

Roger H. Cayton, Malcolm H. Chisholm,* John C. Huffman, and Emil B. Lobkovsky

Contribution from the Department of Chemistry and Molecular Structure Center, Indiana University, Bloomington, Indiana 47405. *Received April 16, 1991*

Abstract: Tetranuclear compounds of formula $[M_2(O_2C\text{-}t\text{-}Bu)_3]_2(\mu\text{-}L)$, where M = Mo and W, have been prepared by either the reaction between $M_2(O_2C\text{-}t\text{-}Bu)_4$ and a dicarboxylic acid or from the reaction between $M_2(O_2C\text{-}t\text{-}Bu)_3(CH_3CN)_x^+$ and an anionic bridging ligand, L(2-). Specific complexes studied are for L = oxalate, perfluoroterephthalate, 1,8-anthracenedicarboxylate, 9,10-dihydro-1,8-anthracenedicarboxylate, 1,1'-ferrocenedicarboxylate, 2,3-dioxyquinoxaline, and 2,7-dioxynaphthyridine. Within this class the M$\frac{4}{}$M bonds are covalently linked by the rigid bridges L in either a perpendicular or parallel mode as represented by oxalate and 1,8-anthracenedicarboxylate, respectively. These complexes have been studied by NMR spectroscopy, UV-visible spectroscopy, cyclic voltammetry, X-ray diffraction (L = 2,7-dioxynaphthyridine), and approximate MO calculations employing the Fenske-Hall method. The oxidized radical cations have been prepared for L = oxalate and perfluoroterephthalate, and these were studied by ESR and near-IR spectroscopy. Collectively these studies show that the electronic coupling between the two quadruply bonded M_2 centers can be mediated by the ligand bridge to yield class I, II, or III behavior in both the perpendicular and parallel modes. In the absence of a suitable ligand bridge, the alignment of the M_2 units in the parallel mode does not favor electronic coupling, and MO calculations reveal little splitting of the δ orbitals. These results are compared with studies of ligand bridged dinuclear systems such as $Ru^{II/III}$-pyrazine-$Ru^{II/III}$ and are discussed in terms of perpendicular and parallel stiff-chain polymers incorporating M$\frac{4}{}$M bonds.

Introduction

The synthesis and reactivity of compounds containing metal-metal multiple bonds have been extensively studied over the past 25 years.[1] Research has focused on the *molecular* chemistry of discrete dinuclear species, and little is known concerning the potential *macromolecular* chemistry of this class of compounds. We have recently initiated an effort aimed toward the synthesis of low-dimensional materials containing metal-metal multiple bonds wherein cooperative interaction among the metal centers at the molecular level may give rise to tunable physical properties (optical, magnetic, conductive, mesomorphic) in the bulk material.

The known examples of dinuclear metal-metal multiple bonds that have been incorporated within low-dimensional polymeric arrays have been prepared by making use of the empty coordination site in the axial positions of M_2L_8-type compounds. Numerous structural studies of the quadruply bonded complexes, $M_2(O_2CR)_4$ (M = Cr, Mo, W)[1] indicate that these species crystallize to form one-dimensional "laddered" chains sustained by intermolecular M-O interactions. Likewise the complexes $Ru_2(O_2CR)_4Cl$[2-5] and $Re_2(O_2CR)_3Cl_3$[6,7] have been shown to crystallize as infinite "zigzag" chains in which the dinuclear centers are linked by Cl bridges in the axial sites. Bidentate organic bases can also serve as axial bridging units. For example, pyrazine has been used to link $M_2(O_2CMe)_4$ molecules (M = Cr, Cu) through the axial positions to form one-dimensional polymers,[8] and the complexes $Ru_2(O_2CR)_4$ apparently form similar polymeric materials with bases such as pyrazine, phenazine, quinoxaline, and 4,4'-bipyridine, although no structures have been reported.[9] Recently ethylenediamine (along with its methyl-substituted derivatives) and dimethylphosphinoethane have been used to bridge quadruply bonded dimolybdenum centers giving rise to infinite polymer chains.[10,11]

The one feature common to each of the above materials is a relatively weak and substitutionally labile M-L axial bond, consistent with the strong trans influence and trans effect exerted by the metal-metal multiple bond. Hence, the integrity of polymers of this type is jeopardized by the relatively weak M-L_{ax}-M backbone. Indeed, it is limited to the solid state and not present in solution. Consequently we sought to develop a synthetic strategy aimed at the preparation of robust, covalently linked, one-dimensional polymers in which the orientation and electronic coupling of the M-M subunits could be systematically tuned. Structure types I and II below illustrate the perpendicular and parallel orientations, respectively, of the metal-metal multiple bonds with respect to the propagation direction of the polymer.

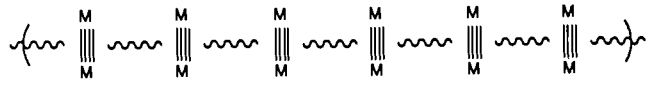

perpendicular

I

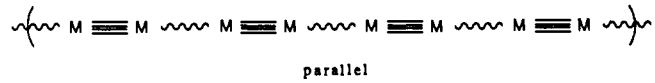

parallel

II

(1) Cotton, F. A.; Walton, R. A. *Multiple Bonds between Metal Atoms*; 1982; John Wiley and Sons.
(2) Bennett, M. J.; Caulton, K. G.; Cotton, F. A. *Inorg. Chem.* **1969**, *8*, 1.
(3) Bino, A.; Cotton, F. A.; Felthouse, T. R. *Inorg. Chem.* **1979**, *18*, 2599.
(4) Martin, D. S.; Newman, R. A.; Vlasnik, L. M. *Inorg. Chem.* **1980**, *19*, 3404.
(5) Togano, T.; Mukaida, M.; Nomura, T. *Bull. Chem. Soc. Jpn.* **1980**, *53*, 2085.
(6) Cotton, F. A.; Gage, L. D.; Rice, C. E. *Inorg. Chem.* **1979**, *18*, 1138.
(7) Kox'min, P. A.; Surazhskaya, M. D.; Larina, T. B.; Bagirov, Sh. A.; Osmanov, N. S.; Kotel'nikova, A. S.; Misailova, T. V. *Sov. J. Coord. Chem.* **1979**, *5*, 1229.
(8) (a) M = Cr: Cotton, F. A.; Felthouse, T. R. *Inorg. Chem.* **1980**, *19*, 328. (b) M = Cu: Morison, B.; Hughes, R. C.; Soos, Z. G. *Acta Crystallogr. B* **1975**, *31*, 762.
(9) Sattelberger, A. P., personal communication.
(10) Eichhorn, B. W.; Kerby, M. C.; Haushalter, R. C.; Vollhardt, K. P. C. *Inorg. Chem.* **1990**, *29*, 723.
(11) Kerby, M. C.; Eichhorn, B. W.; Creighton, J. A.; Vollhardt, K. P. C. *Inorg. Chem.* **1990**, *29*, 1319.

0002-7863/91/1513-8709$02.50/0

In order to gain insight into the potential properties of materials of type I and II, we set out to synthesize suitable oligomeric model systems whose properties could be analyzed by conventional molecular methods. From these we believe we can start to anticipate the electronic communication in the polymers. Herein we describe the synthesis and electronic properties of a series of covalently linked and electronically coupled M–M quadruple-bonded compounds of tungsten and molybdenum having the general structures III and IV, that represent models of subunits for polymer types I and II, respectively.

III IV

The dinuclear subunits employed in this study are the d^4–d^4 dimetal tetracarboxylates of molybdenum and tungsten. The selection of $M_2(O_2CR)_4$ compounds was based upon (1) their available synthesis in multigram quantities, (2) their well-determined ground-state electronic structures and attendant spectroscopies, (3) their tunable redox properties that allow the first oxidation potential to span 2 V as a function of R and M (in several instances the isolation of the radical cation salts $[M_2(O_2CR)_4^+]X^-$ is also possible), and (4) the fairly well-developed substitutional behavior of these complexes and their solvated and substitutionally labile derivatives such as $Mo_2(O_2CR)_2(CH_3CN)_6^{2+}(BF_4^-)_2$.

Preliminary communication of part of this work has appeared.[12]

Results and Discussion

Synthesis. Two strategic approaches have been employed for the synthesis of the linked dinuclear complexes and indeed for the synthesis of higher oligomers. The first takes advantage of the substitutional lability of the $M_2(O_2CR)_4$ compounds with respect to carboxylate group exchange. Specifically a dicarboxylic acid is allowed to react with 2 equiv of $M_2(O_2CR)_4$ in the generalized reaction shown in eq 1.

$$2M_2(O_2CR)_4 + HO_2CR'CO_2H \xrightarrow[\text{toluene}]{\text{rt}} [M_2(O_2CR)_3]_2(\mu\text{-}O_2C\text{-}R'\text{-}CO_2) + 2RCO_2H \quad (1)$$

There are a number of limitations on this type of reaction. (1) It is reversible and therefore the appropriate choice of R and R′ must be made if the linked dinuclear complexes are to be isolated. (2) Higher oligomeric species are also formed in competition with the desired tetranuclear species, and (3) the reaction rate is very sensitive to the substitutional lability of the metal and the M–M electronic configuration. For example, while this procedure works quite well for M = Mo or W, it is not kinetically useful for M = Rh. Changing the concentrations of the dicarboxylic acid and the $M_2(O_2CR)_4$ complex in eq 1 to a 1:1 mole ratio favors synthesis of the polymer by condensation reactions involving the linked tetranuclear complexes and their higher oligomers with elimination of further RCO_2H.

The second strategy involves the use of a cationic complex of formula $M_2(O_2CR)_3^+X^-$ supported by substitutionally labile solvent ligands. Such complexes were not known for M = Mo and W, so we prepared one example from the ligand comproportionation reaction shown in eq 2. The related complex $Mo_2(O_2CMe)_2(CH_3CN)_6^{2+}(BF_4^-)_2$ had been previously prepared and well-characterized.[13]

$$Mo_2(O_2C\text{-}t\text{-}Bu)_4 + Mo_2(O_2C\text{-}t\text{-}Bu)_2(CH_3CN)_6^{2+}(BF_4^-)_2 \xrightarrow[CH_3CN]{\text{rt}} 2[Mo_2(O_2C\text{-}t\text{-}Bu)_3(CH_3CN)_x^+(BF_4^-)] \quad (2)$$

Reaction 2 is in fact an equilibrium reaction, and isolation of the desired $Mo_2(O_2C\text{-}t\text{-}Bu)_3^+$-containing salt rests on its favorable equilibrium position ca. 1:1:6 at 22 °C, and on one's ability to separate it from the other species present in eq 2. At lower temperatures the disproportionation of the $Mo_2(O_2C\text{-}t\text{-}Bu)_3^+$ containing salt is not rapid relative to its reaction to form the linked tetranuclear complexes by the reaction outlined in 3.

$$2Mo_2(O_2C\text{-}t\text{-}Bu)_3^+(BF_4^-) + (M^+)_2\text{bridge}^{2-} \xrightarrow[THF]{0\ ^\circ C} [Mo_2(O_2C\text{-}t\text{-}Bu)_3]_2(\text{bridge}) + 2MBF_4 \quad (3)$$

An idealized synthesis for a polymer involving this strategy utilizes the $M_2(O_2CR)_2^{2+}$-containing salts as shown in eq 4.

$$M_2(O_2CR)_2^{2+}(BF_4^-)_2 + (M^+)_2\text{bridge}^{2-} \xrightarrow[CH_3CN/THF]{} 1/n[M_2(O_2CR)_2(\text{bridge})]_n + 2MBF_4 \quad (4)$$

Dicarboxylate-Linked M_4 Systems. By exploiting the lesser solubility of the dicarboxylate-bridged compounds formed in reaction 1 and with the use of toluene as a solvent, the M_4-containing complexes precipitate from solution. In all cases reported here the linked M_4 complexes are soluble in THF which allows separation from any higher oligomers. Consequently synthesis of polymers can be carried out in THF, DMF, or similar more polar solvents.

Whereas the $M_2(O_2CR)_4$ compounds are yellow when R = alkyl, the linked M_4 complexes range in color from yellow to blue and the polymers are in general more intensely colored, and their spectra red-shifted when compared to their respective M_4 complexes. For example, the $[W_2(O_2C\text{-}t\text{-}Bu)_3]_2$(oxalate) complex is blue, and the tungsten oxalate polymer is deep purple.

2,7-Dioxynaphthyridine- and 2,3-Dioxyquinoxaline-Bridged M_4 Complexes. The dianions derived from 2,7-dihydroxynaphthyridine and 2,3-dihydroxyquinoxaline have been used in reactions based on eq 3 for the preparation of ON-linked M_4 complexes.

A summary of the M_4 complexes synthesized and characterized in this study is given in Table I, and full details are included in the Experimental Section or elsewhere in this paper.

Oxidized M_4 Systems. The radical cations that have been prepared according to the general reaction shown in eq 5 are also listed in Table I.

$$[M_2(O_2CR)_3]_2(\text{bridge}) + OX \xrightarrow[THF]{} [M_2(O_2CR)_3]_2(\text{bridge})^{\bullet+} + RED \quad (5)$$

where

$$OX = AgPF_6 \text{ or } Cp_2FeBF_4 \text{ and } RED = Cp_2Fe \text{ or } Ag(m)$$

Stability of the M_4 Complexes. The synthetic utility of the preparation of a polymer incorporating M_2 subunits is clearly limited by the integrity or kinetic persistence of the skeletal M–L bonds. Within this context the stability of the M_4 complexes is particularly noteworthy. Of the syntheses utilizing dicarboxylic acids (eq 1) only the products containing the oxalate and $p\text{-}C_6F_4(CO_2)_2$ bridges proved to be stable (kinetically persistent) M_4 complexes. Other dicarboxylate ligands that could potentially link M_2 units in a perpendicular manner (e.g., fumarate, acetylene dicarboxylate, terephthalate) were found to yield M_4 species that readily decomposed in solution via ligand disproportionation reactions. There is ample precedent for such behavior based upon the known chemistry of the $M_2(O_2CR)_4$ subunits. (1) For M = Mo and W the carboxylate ligands are substitutionally labile. For example, an equimolar solution of $Mo_2(O_2C\text{-}t\text{-}Bu)_4$ and $Mo_2(O_2CCH_2\text{-}t\text{-}Bu)_4$ in C_6D_6 quickly affords the complete series of scrambled species, $Mo_2(O_2C\text{-}t\text{-}Bu)_n(O_2CCH_2\text{-}t\text{-}Bu)_{4-n}$ where n = 0–4.[14] (2) Thermodynamically, replacement of an O_2CR group in $M_2(O_2CR)_4$ by O_2CR' is favorable only when the electron-withdrawing ability of R′ ≫ R, i.e., the pK_a of $R'CO_2H$, is less

(12) Cayton, R. H.; Chisholm, M. H. *J. Am. Chem. Soc.* **1989**, *111*, 8921. Cayton, R. H.; Chisholm, M. H.; Huffman, J. C.; Lobkovsy, E. B. *Angew. Chem., Intl. Ed. Engl.* **1991**, *30*, 862.

(13) (a) Cotton, F. A.; Reid, A. H., Jr.; Schwotzer, W. *Inorg. Chem.* **1985**, *24*, 3965. (b) Garner, C. D.; Clegg, W.; Pimblett, G. *J. Chem. Soc., Dalton Trans.* **1986**, 1257.

(14) Casas, J. M.; Cayton, R. H.; Chisholm, M. H. *Inorg. Chem.* **1991**, *30*, 358.

Table I. Summary of Tetranuclear Complexes Depicting their Proposed Structures and Giving the Abbreviated Names and Colors

Compound	Metal	Name	Color
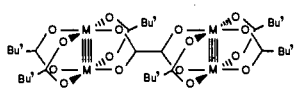	Mo	Mo_4(OXA)	Red
	W	W_4(OXA)	Blue
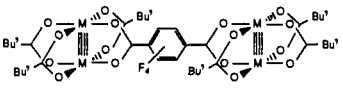	Mo	Mo_4(PFT)	Orange
	W	W_4(PFT)	Blue
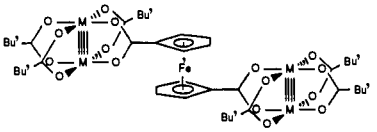	W	W_4(FDC)	Maroon
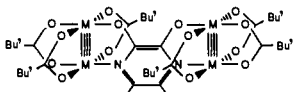	Mo	Mo_4(DOQ)	Orange
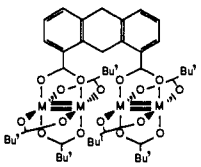	Mo	Mo_4(DAND)	Yellow
	W	W_4(DAND)	Red
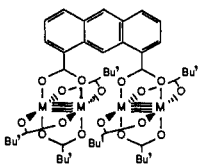	Mo	Mo_4(AND)	Orange
	W	W_4(AND)	Green
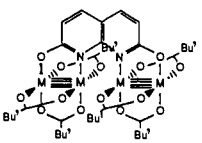	Mo	Mo_4(DON)	Orange
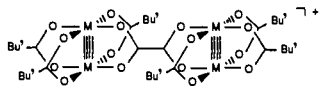	Mo (BF_4^-)	$Mo_4(OXA)^+$	Maroon
	W (BF_4^-)	$W_4(DXA)^+$	Blue
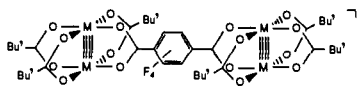	Mo (PF_6^-)	$Mo_4(PFT)^+$	Orange
	W (BF_4^-)	$W_4(PFT)^+$	Blue

than RCO_2H.[15] (3) An M_4 complex linked in the perpendicular mode does not allow for axial ligation (the importance of which will be discussed later). Interestingly, a stable perpendicular-linked M_4 complex was obtained for the functionalized bridge 1,1′-ferrocenedicarboxylate, eq 6. The mixed-metal product is inert toward further ligand redistribution reactions and in solution thus represents a technique that may prove useful for the incorporation of dopants directly within the polymer backbone.

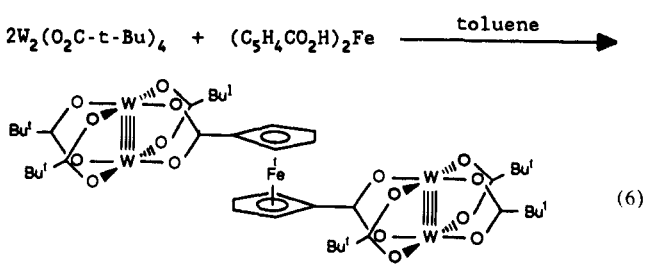

(6)

(15) See, for example: Cotton, F. A.; Falvello, L. R.; Reid, A. H., Jr.; Tocher, J. H. *J. Organomet. Chem.* **1987**, *319*, 87.

Scheme I

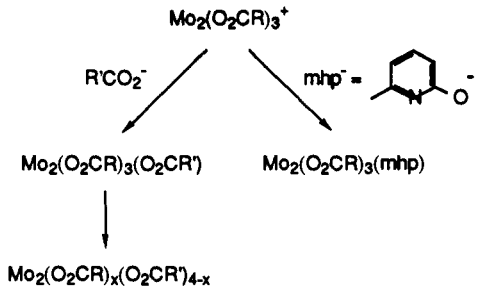

By contrast, the dicarboxylate-bridged M_4 systems linked in the parallel mode tend to be more stable (kinetically persistent) when the spanning unit is 1,8-anthracenedicarboxylate or 9,10-dihydro-1,8-anthracenedicarboxylate. This stability is likely due to the favorable axial M–O interactions set up by the 1,8-substituted anthracene moiety as shown in V. Consistent with this explanation, the M_4 complex derived from the 1,5-anthracenedicarboxylate bridge that lacks axial M–O interactions (see VI below) is kinetically labile in solution. The strength of these axial interactions will be addressed in greater detail during the discussion of their NMR behavior.

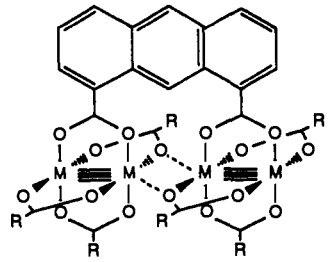

V

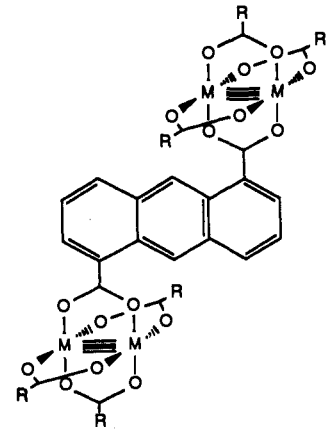

VI

The NO linked M_4 complexes exhibit kinetic inertness in both the perpendicular (2,3-dioxyquinoxaline) and parallel (2,7-dioxynaphthyridine) linked modes. In these complexes the M_2 cores are supported by both carboxylate and α-oxypyridine ligands and as such appear not to undergo the ligand exchange reactions so prevalent with mixed carboxylate M_2 subunits. The kinetic inertness of this group of bridged complexes may well indicate thermodynamic stability—but this is not proven. Indeed, mixed ligand dinuclear complexes of the general formula $Mo_2(O_2CR)_3(L)$ can be prepared wherein L represents either an α-oxypyridine ligand or a carboxylate group as shown in Scheme I. However, only the α-oxypyridine complexes exhibit kinetic inertness in solution; the mixed carboxylate complexes readily undergo ligand scrambling.

Structures of M_4 Complexes. To date only one complex has yielded crystals suitable for a single-crystal X-ray study. However, with this fully characterized molecule and the solution NMR data for related complexes we feel confident in claiming the synthesis

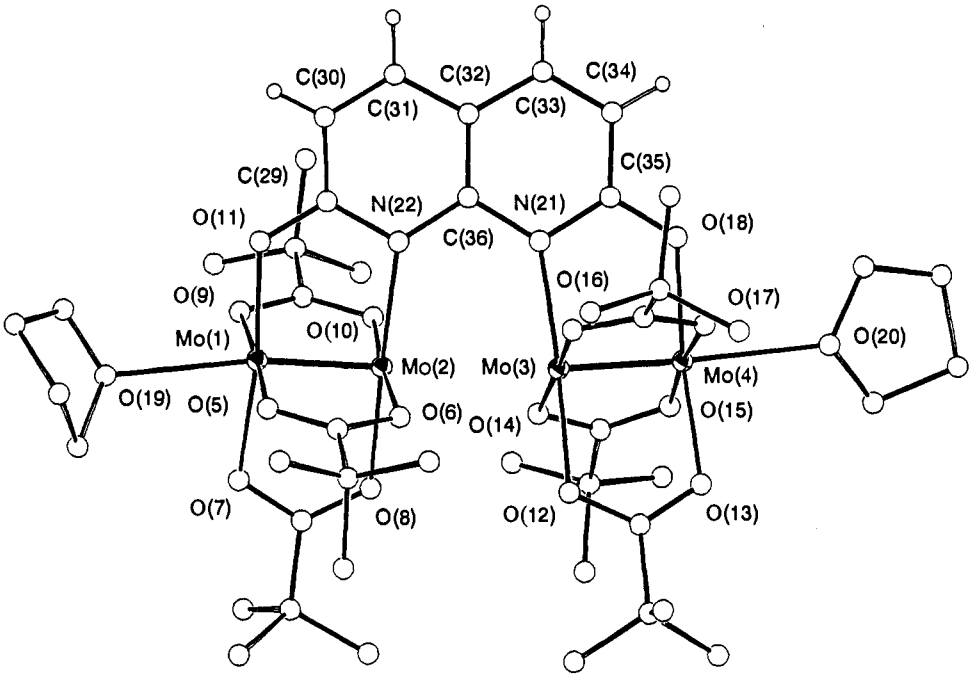

Figure 1. Ball-and-stick drawing of the $[Mo_2(O_2C\text{-}t\text{-}Bu)_3]_2(\mu\text{-}2,7\text{-}O_2N_2C_8H_4)\cdot 2THF$ molecule, $Mo_4(DON)$, giving the atom number scheme used in the tables. This view is roughly perpendicular to the plane of the bridging ligand and emphasizes the parallel alignment of the M≡M bonds.

Table II. Selected Interatomic Distances (Å) for $Mo_4(DON)$ with Estimated Standard Deviations in Parentheses

Mo(1)-Mo(2)	2.0960 (3)	O(11)-C(29)	1.2956 (2)
Mo(1)-O(5)	2.1233 (4)	O(18)-C(35)	1.2987 (2)
Mo(1)-O(7)	2.1108 (4)	N(21)-C(35)	1.3819 (3)
Mo(1)-O(9)	2.1045 (4)	N(21)-C(36)	1.3924 (2)
Mo(1)-O(11)	2.0626 (4)	N(22)-C(29)	1.3828 (2)
Mo(1)-O(19)	2.5596 (4)	N(22)-C(36)	1.3775 (3)
Mo(1)-O(6)	2.1126 (4)	C(29)-C(30)	1.4184 (3)
Mo(2)-O(8)	2.1278 (4)	C(30)-C(31)	1.3548 (2)
Mo(2)-O(10)	2.1083 (4)	C(31)-C(32)	1.4206 (2)
Mo(2)-N(22)	2.1871 (4)	C(32)-C(33)	1.4153 (3)
Mo(3)-Mo(4)	2.0963 (3)	C(32)-C(36)	1.3882 (3)
Mo(3)-O(12)	2.1222 (5)	C(33)-C(34)	1.3564 (2)
Mo(3)-O(14)	2.1079 (4)	C(34)-C(35)	1.4166 (3)
Mo(3)-O(16)	2.1238 (4)	Mo(2)-Mo(3)	3.171 (1)
Mo(3)-N(21)	2.1682 (5)	Mo(2)-O(14)	2.814 (5)
Mo(4)-O(13)	2.1134 (4)	Mo(3)-O(6)	2.841 (6)
Mo(4)-O(15)	2.1102 (4)		
Mo(4)-O(17)	2.1050 (4)		
Mo(4)-O(18)	2.0662 (4)		
Mo(4)-O(20)	2.4943 (4)		

of prototypical parallel and perpendicular-linked species.

$[Mo_2(O_2C\text{-}t\text{-}Bu)_3]_2(\mu\text{-}2,7\text{-}O_2N_2C_8H_4)$. A ball-and-stick drawing of the 2,7-dioxynaphthyridine-bridged complex is shown in Figure 1. This view is roughly perpendicular to the M_4 chain, and a view down the chain is given in Figure 2. Selected bond distances and angles are given in Tables II and III, respectively.

The metal–metal distances alternate along the Mo_4 chain as short, 2.10 Å, long, 3.17 Å, and short, 2.10 Å, corresponding formally to two localized Mo–Mo quadruple bonds brought in close proximity through the agency of the 2,7-dioxynaphthyridine bridge. There is a twisting of the naphthyridine ligand as can be clearly seen from inspection of Figure 2. This leads to a Mo–Mo–Mo angle of 149° and allows for the internal Mo atoms to bond to oxygen atoms of their neighboring μ-carboxylate ligands, Mo–O = 2.81 and 2.84 Å. In addition, the ends of the Mo_4 chain are terminated with THF ligands, Mo–O(THF) = 2.53 (2) Å (av). On the basis of the structure of this molecule we can anticipate what a higher oligomer might look like. We envisage a chain in which Mo_2 units are linked in a ruffled array such that in the solid state these $Mo_2(\mu\text{-}O)_2$ interactions can be maintained, as indeed are found in the solid-state laddered structures of

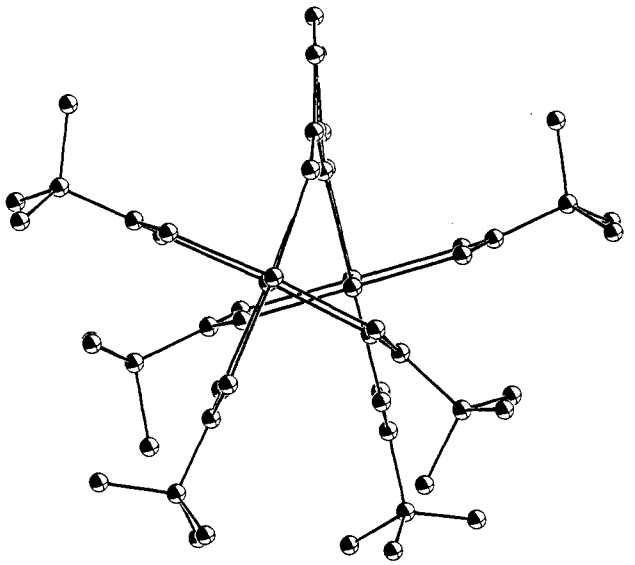

Figure 2. A ball-and-stick drawing of the $Mo_4(DON)\cdot 2THF$ molecule looking down the Mo_4 chain and parallel to the plane of the bridging ligand. This view emphasizes the twist of the bridging ligand and reveals the displacement of each Mo≡Mo unit from the idealized linear M_4 arrangement. The THF ligands were omitted for clarity.

$[M_2(O_2CR)_4]_\infty$ complexes and in their liquid crystalline phases.[16]

Solution NMR Studies. The ^1H NMR spectra of the 2,7-dioxynaphthyridine-bridged complex, $Mo_4(DON)$, whose structure has just been described, are temperature-dependent and are qualitatively very similar to the 1,8-anthracenedicarboxylate-bridged complexes, $M_4(AND)$, and the 9,10-dihydro-1,8-anthracenedicarboxylate-bridged complexes, $M_4(DAND)$, where M = Mo and W. Specifically at room temperature in THF-d_8

(16) Cayton, R. H.; Chisholm, M. H.; Darrington, F. D. *Angew. Chem., Int. Ed. Engl.* **1990**, *29*, 1481. Several other $M_2(O_2CR)_4$ compounds where M = Cu, Rh, and Ru have been shown to exhibit thermotropic discotic mesophases and these have been extensively studied by Giroud-Godquin and co-workers at Grenoble. For a recent review of these and related metallomesogens see Giroud-Godquin, A. M.; Maitlis, P. M. *Angew. Chem., Int. Ed. Engl.* **1991**, *30*, 375.

Table III. Selected Interatomic Angles (deg) for Mo_4(DON)

A	*B*	*C*	angle
Mo(2)	Mo(1)	O(5)	91.113 (16)
Mo(2)	Mo(1)	O(7)	92.450 (15)
Mo(2)	Mo(1)	O(9)	91.837 (15)
Mo(2)	Mo(1)	O(11)	94.052 (15)
Mo(2)	Mo(1)	O(19)	170.8060 (20)
Mo(1)	Mo(2)	O(6)	92.350 (15)
Mo(1)	Mo(2)	O(8)	90.791 (15)
Mo(1)	Mo(2)	O(10)	91.957 (16)
Mo(1)	Mo(2)	N(22)	91.664 (15)
Mo(4)	Mo(3)	O(12)	91.311 (15)
Mo(4)	Mo(3)	O(14)	91.589 (15)
Mo(4)	Mo(3)	O(16)	91.795 (15)
Mo(4)	Mo(3)	N(21)	92.455 (15)
Mo(3)	Mo(4)	O(13)	92.311 (15)
Mo(3)	Mo(4)	O(15)	91.739 (15)
Mo(3)	Mo(4)	O(17)	92.202 (15)
Mo(3)	Mo(4)	O(18)	92.991 (15)
Mo(3)	Mo(4)	O(20)	176.4300 (10)
Mo(1)	O(11)	C(29)	120.347 (13)
Mo(4)	O(18)	C(35)	120.581 (14)
Mo(3)	N(21)	C(35)	113.759 (13)
Mo(3)	N(21)	C(36)	126.980 (13)
Mo(2)	N(22)	C(29)	114.138 (12)
Mo(2)	N(22)	C(36)	128.109 (12)
C(35)	N(21)	C(36)	117.502 (12)
C(29)	N(22)	C(36)	117.146 (11)
O(11)	C(29)	N(22)	119.062 (11)
O(11)	C(29)	C(30)	118.515 (13)
N(22)	C(29)	C(30)	122.407 (12)
C(29)	C(30)	C(31)	118.574 (13)
C(30)	C(31)	C(32)	120.656 (11)
C(31)	C(32)	C(33)	121.949 (11)
C(31)	C(32)	C(36)	118.365 (13)
C(33)	C(32)	C(36)	119.585 (13)
C(32)	C(33)	C(34)	119.602 (11)
C(33)	C(34)	C(35)	119.758 (13)
O(18)	C(35)	N(21)	118.176 (12)
O(18)	C(35)	C(34)	120.005 (13)
N(21)	C(35)	C(34)	121.505 (13)
N(21)	C(36)	N(22)	116.254 (11)
N(21)	C(36)	C(32)	121.319 (12)
N(22)	C(36)	C(32)	122.427 (12)
Mo(1)	Mo(2)	Mo(3)	149.96 (9)
Mo(2)	Mo(3)	Mo(4)	148.10 (9)
Mo(1)	Mo(2)	O(14)	164.74 (61)
Mo(4)	Mo(3)	O(6)	166.10 (68)

there are two types of carboxylate ligands in the integral ratio 2:1 assignable to carboxylates that are cis and trans, respectively, to the bridging ligands. However, at low temperature we do observe three types of carboxylates as expected for a structure of C_2 symmetry that allows for $M_2(-O)_2$ interaction as found in the solid state for Mo_4(DON). We suggest that the room-temperature behavior is indicative of a fluxional molecule in which enantiomers interconvert via a C_{2v} transition state. This process is shown below in VII.

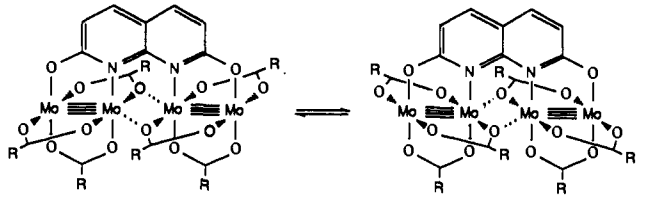

VII

The coalescence behavior of the O_2C-*t*-Bu ligands reflects the magnitude of the $M_2(\mu\text{-}O)_2$ interactions ca. T_c = −50 °C for Mo_4(DON), T_c = −80 °C for Mo_4(AND) and Mo_4(DAND), and T_c < −100 °C for W_4(AND) and W_4(DAND). The lower T_c values for the W_4 complexes correlate with the weaker axial binding of oxygen donor ligands to W—W carboxylates.[17] Thus we feel confident in claiming that the anthracene and 9,10-dihydroanthracene species have the structure shown in V. It is interesting to note that the geminal protons in the 9,10-positions of the anthracene ring of the M_4(DAND) complexes remain nondiastereotopic even at −100 °C, although some broadening of these singlets is observed at this temperature. This implies that the folding of the two aromatic rings that is brought about by the tetrahedral carbon atoms C9 and C10 must be flapping rapidly on the NMR time scale leading to a time-averaged planar C_{14} skeleton.

Finally we note that although we believe that the anthracene- and naphthyridine-bridged M_4 complexes adopt similar M_4 chains in the ground state due to the weak $M_2(\mu\text{-}O)_2$ interactions, their dynamic behavior is somewhat different. Specifically the 2,7-dioxynaphthyridine-bridged compound will have to undergo a sliding or skating motion which leads to an effective enantiomerization of the two possible C_2 ground-state geometries. This is shown diagrammatically in VIII below. By contrast, in the anthracene- and 9,10-dihydroanthracene-linked carboxylates the M_2 units swivel about the carboxylate-CO_2 carbon-to-ring single bond in a concerted motion as shown schematically by IX.

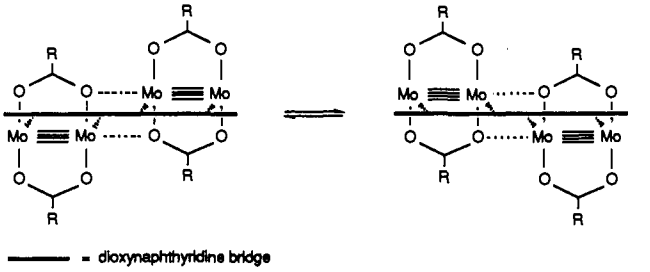

VIII

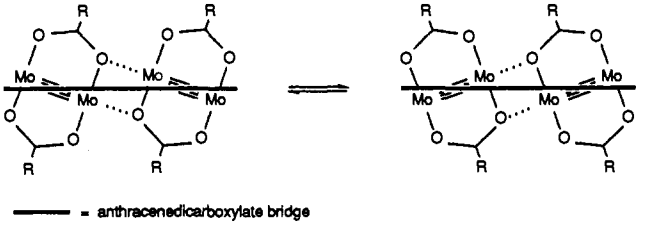

IX

Either of the motions described above and depicted by VIII and IX would lead to a polymer maintaining a parallel alignment of M_2 units.

Oxalate- and Perfluoroterephthalate-Bridged Compounds. The ^{1}H NMR spectra of these compounds show only two types of carboxylate ligands in the integral ratio 1:2 as expected for a perpendicular-linked M_4 dimer. Regretably we have not obtained crystals suitable for single-crystal X-ray studies. We cannot therefore be sure that the M_4 atoms all lie in the same plane. In the case of μ-oxalate M_4-containing compounds we feel this is likely to be the case because of the favorable π-interactions. The free oxalate ligand is planar and the interaction with the M_2 δ orbitals described later would do nothing to disturb this planarity. In the case of the perfluoroterephthalate-linked complex the CO_2 planes would almost certainly be twisted from that of the phenyl ring as seen, for example, in the solid-state structure of $Mo_2(O_2CPh)_4$.[18] There is, however, still a tendency for the CO_2 and phenyl π-system to want to couple in $M_2(O_2CAr)_4$ complexes as evidenced by the red-shifting of the M_2 δ-to-CO_2 π^* electronic transition.[19] The net effect is that the two M_2 units would

(17) Compare, for example: $W_2(O_2CEt)_4$ where $W\text{–}O_{ax}$ = 2.665 (4), Chisholm, M. H.; Chiu, H. T.; Huffman, J. C. *Polyhedron* **1984**, *3*, 759. $Mo_2(O_2CMe)_4$ where $Mo\text{–}O_{ax}$ = 2.645 (4), Cotton, F. A.; Mester, Z. C.; Webb, T. R. *Acta Crystallogr.* **1974**, *B30*, 2768.

(18) Cotton, F. A.; Extine, M.; Cage, L. D. *Inorg. Chem.* **1978**, *17*, 172.

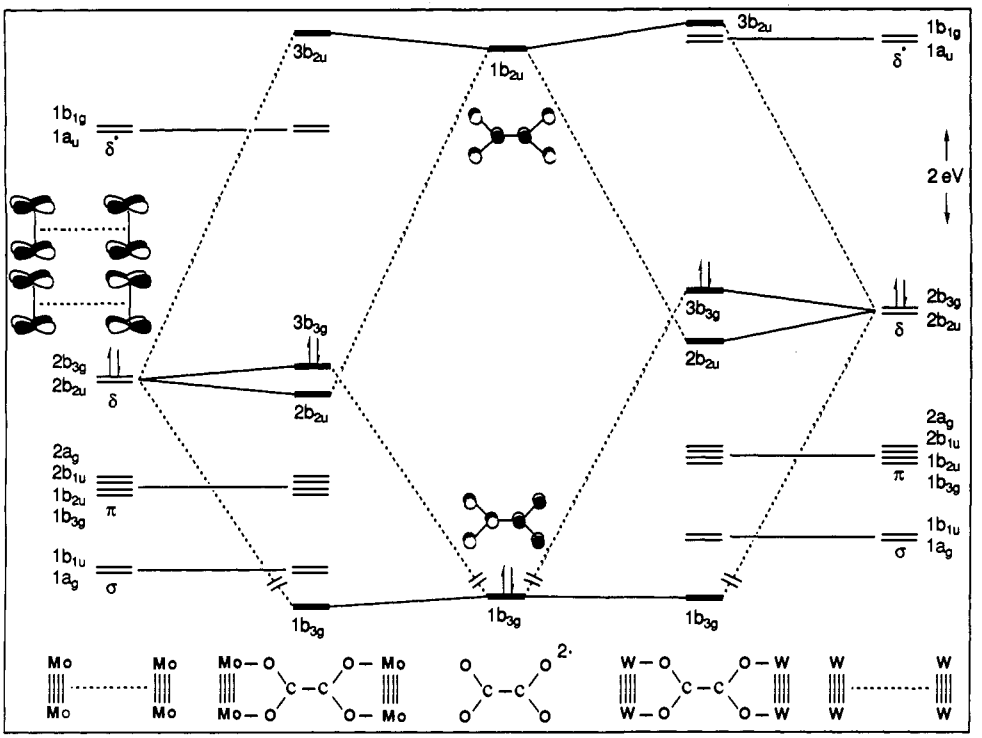

Figure 3. An orbital interaction diagram showing the formation of $M_4(\mu$-oxalate) from the frontier orbitals of two M_2 fragments and oxalate. The two M_2 fragments yield isoenergetic in- and out-of-phase δ orbitals that mix with the oxalate HOMO and LUMO orbitals of π symmetry. The interactions on the left are for molybdenum and those on the right are for tungsten. The arrows indicate the HOMO of each fragment.

probably be twisted with respect to each other as shown in X. As defined earlier by I, the polymer derived from such a coupling would have its propagating axis perpendicular to the M–M axes.

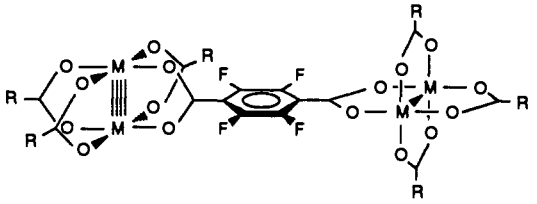

X

$[W_2(O_2C$-t-$Bu)_3]_2(\mu$-$(O_2CC_5H_4)_2Fe)$. In the ferrocenyl-bridged compound the description of perpendicular and parallel coupling becomes ambiguous. First of all there is the question of the relative twist of the CO_2 groups with respect to the plane of the cyclopentadienyl C_5 ring. Second, there is the question of the disposition of the two substituted cyclopentadienyl ligands. As shown in Table I these are disposed such that there is a center of inversion to the molecule and the two W_2 units remain well separated. However, it is possible to envisage a ground-state structure wherein the two W_2 units align themselves in a parallel manner akin to that of the anthracene-bridged species so that axial M–O interactions are available as shown in XI.

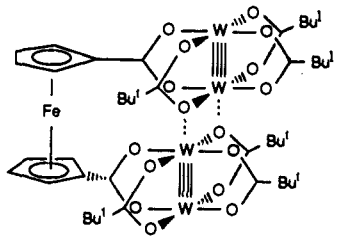

XI

(19) (a) For $Mo_2(O_2CPh)_4$, see: San Filippo, J.; Snaidoch, H. J. *Inorg. Chem.* **1976**, *15*, 2209. (b) For $W_2(O_2CPh)_4$, see: Cotton, F. A.; Wang, W. *Inorg. Chem.* **1984**, *23*, 1604.

Bonding Considerations. Electronic Coupling of M_2 Subunits in M_4 Complexes. These M_4 complexes lend themselves to the types of computational procedures that have proven so insightful in the elucidation of the electronic structures of M–M multiply bonded systems. The insight provided by such techniques for an M_4 molecule may in turn be useful in sensing the electronic properties of the $[M_2]_n$ polymers.

Considering first the individual M_2 subunits, the electronic structures of the d^4–d^4 $M_2(O_2CR)_4$ (M = Cr, Mo, W) series have been extensively examined at numerous computational levels.[20] Each of these compounds has been shown to possess a $\sigma^2\pi^4\delta^2$ electron configuration wherein the M–M δ interaction is the HOMO and the δ^* orbital is the LUMO for R = H or alkyl, regardless of the nature of the metal centers. The lowest energy unoccupied ligand-based orbital (O_2CR π^*) was found to reside at higher energy than the M–M δ^* orbital, and, furthermore, the energetic separation between these virtual orbitals was found to vary according to the trend Cr $\gg$ Mo > W.

Perpendicularly Linked Systems. Fenske–Hall type molecular orbital calculations[21] were carried out on the model oxalate-bridged species $[M_2(O_2CH)_3]_2(\mu$-$O_2CCO_2)$, M = Mo, W, $M_4(OXA)'$ wherein formate ligands have been used in place of the t-Bu carboxylate groups for reasons of computational simplicity. Details of the atomic coordinates and calculational technique are provided in the Computational Procedures in the Experimental Section.

We begin by considering the electronic structure of the model oxalate-bridged molybdenum complex, $Mo_4(OXA)'$, under D_{2h} symmetry. The frontier orbital picture of this compound is constructed by a fragment approach wherein the oxalate bridge

(20) (a) Norman, J. G., Jr.; Kolari, H. J. *J. Chem. Soc., Chem. Commun.* **1975**, 649. (b) Norman, J. G., Jr.; Kolari, H. J.; Gray, H. B.; Trogler, W. C. *Inorg. Chem.* **1977**, *16*, 987. (c) Benard, M. *J. Am. Chem. Soc.* **1978**, *100*, 2354. (d) Benard, M.; Veillard, A. *Nouv. J. Chim.* **1977**, *1*, 97. (e) Cotton, F. A.; Stanley, G. G. *Inorg. Chem.* **1977**, *16*, 2668. (f) Guest, M. F.; Hillier, I. H.; Garner, C. D. *Chem. Phys. Lett.* **1977**, *48*, 587. (g) Braydich, M. D.; Bursten, B. E.; Chisholm, M. H.; Clark, D. L. *J. Am. Chem. Soc.* **1985**, *107*, 4459. (h) Bursten, B. E.; Clark, D. L. *Polyhedron* **1987**, *6*, 695. (i) Manning, M. C.; Holland, G. F.; Ellis, D. E.; Trogler, W. C. *J. Phys. Chem.* **1983**, *87*, 3083. (j) Ziegler, T. *J. Am. Chem. Soc.* **1985**, *107*, 4453. (k) Atha, P. M.; Hillier, I. H.; Guest, M. F. *Mol. Phys.* **1982**, *46*, 437.

(21) Hall, M. B.; Fenske, R. F. *Inorg. Chem.* **1972**, *11*, 768.

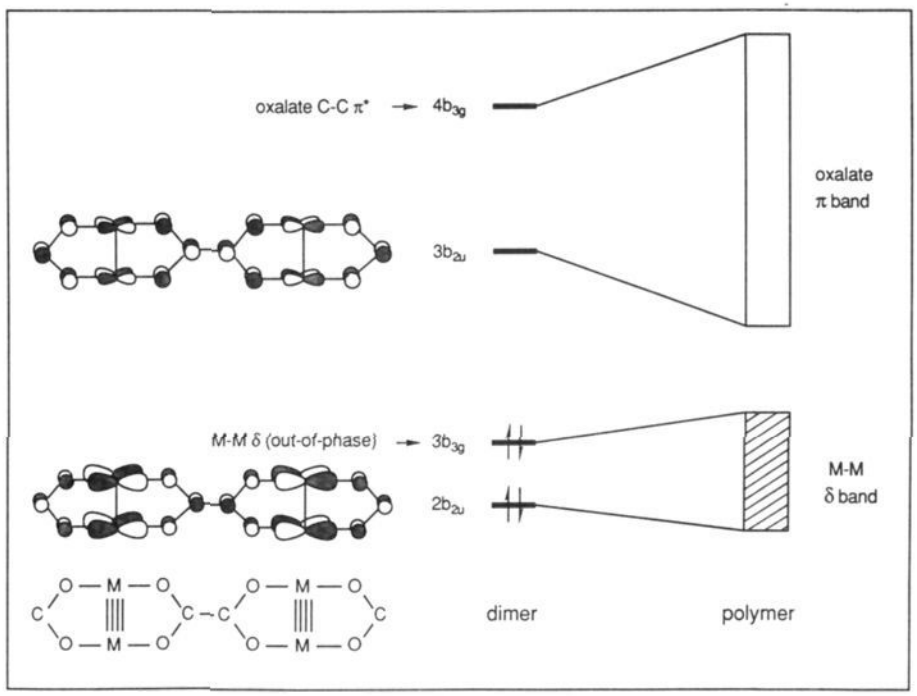

Figure 4. Qualitative diagram depicting the formation of the δ and oxalate based bands in a 1-D perpendicular oxalate bridged polymer.

is allowed to interact with two Mo$\overset{4}{-}$Mo moieties. The resulting interaction diagram is illustrated on the left side of Figure 3. On the extreme left are shown the Mo-based orbitals of two Mo–Mo quadruple bonds separated by ca. 7.0 Å. At this distance there is negligible interaction between the metal-based orbitals of the two Mo_2 units, hence the respective Mo–Mo σ, π, and δ orbitals form essentially degenerate sets. The two LUMOs are the Mo–Mo δ* combinations, while the lowest energy empty ligand-based orbital (HCO_2 π*) is found to lie higher in energy and is not shown on the diagram. When these two Mo$\overset{4}{-}$Mo moieties are linked with an oxalate bridge a unique bonding picture emerges. Only two $C_2O_4^{2-}$ fragment orbitals ($1b_{3g}$, $1b_{2u}$) interact appreciably with the Mo$\overset{4}{-}$Mo manifold, and these are depicted in the center of Figure 3. The lower energy $C_2O_4^{2-}$ orbital of b_{3g} symmetry interacts weakly with one of the Mo–Mo δ combinations causing the latter to be slightly destabilized due to the filled–filled nature of the interaction. The empty b_{2u} oxalate orbital is involved in a more significant interaction with the other Mo–Mo δ combination such that this occupied metal-based orbital is stabilized in energy. The net result is a splitting of the two Mo–Mo δ orbitals of 0.63 eV. The remaining metal-based frontier orbitals (σ, π, and δ*) are essentially unperturbed by the oxalate π-system. The relatively low energy of the empty oxalate b_{2u} orbital makes it an efficient π-acceptor orbital as evidenced in its increase in electron density from 0.00 e to 0.13 e upon bridging the two Mo_2 units. In this respect, the oxalate ligand provides an electronically unsaturated and energetically favorable bridge for the electronic coupling of the two dinuclear centers.

The interaction diagram for the analogous tungsten system $W_4(OXA)'$ is pictured on the right half of Figure 3. As expected, the tungsten-based orbitals are each located slightly higher in energy than their molybdenum counterparts. This effect causes the b_{3g} interaction to become even weaker resulting in less destabilization of the HOMO (W–W δ orbital, $3b_{3g}$). In contrast, the π-backbonding interaction between the oxalate b_{2u} orbital and the W–W δ b_{2u} combination is greater for tungsten compared to molybdenum. This is due in part to the decreased energetic separation between the b_{2u} orbitals in the case of the tungsten system and in part to a greater overlap with the more diffuse tungsten 5d orbitals ($\langle M\text{–}M2b_{2u}|C_2O_4b_{2u}\rangle$ = 0.055 (M = W), 0.050 (M = Mo)). The result is a greater degree of electron transfer from the M–M δ manifold of tungsten onto the oxalate bridge in the ground state, exemplified by the increase in population of the empty oxalate b_{2u} orbital to 0.20 e upon ligation, cf. 0.13 e for M = Mo as noted above.

The metal-to-bridging ligand π-backbonding inherent in the above oxalate-linked tetranuclear systems is qualitatively analogous to that found in the now classic pyrazine-linked dinuclear complexes of Taube et al. (i.e., $[(NH_3)_5M]_2(pyz)^{4+}$, M = Ru, Os).[22] The pyrazine ligand possesses a low-lying empty π-type orbital that serves as an efficient π-acceptor orbital with the t_{2g}^6 metal centers in octahedral Ru^{II} and Os^{II} complexes.

The calculated energy of the oxalate-based $3b_{2u}$ orbital of the $M_4(OXA)'$ model complexes warrants further comment. The calculations indicate that the $3b_{2u}$ orbital lies at slightly higher energy than the M–M δ* orbitals for both the molybdenum and tungsten species (see Figure 3). It is likely that the energy of these $3b_{2u}$ orbitals is biased high, and the actual energy may in fact be lower than the M–M δ* set. The Fenske–Hall method often places ligand-based virtual orbitals too high in energy. For example, in $Mo_2(O_2CH)_4$ the lowest energy empty HCO_2 π*-type orbital is calculated by the Fenske–Hall method to be ca. 5.8 eV higher in energy than would be expected based on the electronic spectra of $Mo_2(O_2CR)_4$ compounds.[23] Furthermore, the electronic spectra of the tetranuclear complexes reported here (see next section) are also consistent with a μ-dicarboxylate-based LUMO, rather than a metal-based δ*-type LUMO.

Although we have not carried out calculations on other perpendicularly linked systems, we anticipate that the electronic coupling will only be possible when the M_2 δ and CO_2 π/π* systems are coupled through the agency of a ligand-bridged π system such as C≡C, C=C, or phenyl. For a polymer this M_2 δ/CO_2 bridge coupling will lead to the formation of valence and conduction bands as shown schematically in Figure 4. We anticipate that the polymers will range from insulating to semiconducting, to conducting, with the band-gap reflecting the degree

(22) (a) Richardson, D. E.; Taube, H. *Coord. Chem. Rev.* **1984**, *60*, 107. (b) Creutz, C.; Taube, H. *J. Am. Chem. Soc.* **1969**, *91*, 3988. (c) Creutz, C.; Taube, H. *J. Am. Chem. Soc.* **1973**, *95*, 1086. (d) Magnuson, R. H.; Lay, P. A.; Taube, H. *J. Am. Chem. Soc.* **1983**, *105*, 2507. (e) Bino, A.; Lay, P. A.; Taube, H.; Wishart, J. F. *Inorg. Chem.* **1985**, *24*, 3969. (f) See, also: Creutz, C. *Prog. Inorg. Chem.* **1983**, *30*, 1.

(23) Cayton, R. H.; Chisholm, M. H., unpublished results.

Table IV. Electronic Absorption Data for the Series of Tetranuclear Complexes $[M_2(O_2C\text{-}t\text{-}Bu)_3]_2$(bridge) and Dinuclear Compounds $M_2(O_2C\text{-}t\text{-}Bu)_4$ (M = Mo, W)

compound[a]	λ_{max} (nm)	λ_{max} (cm^{-1})	ϵ (M^{-1} cm^{-1})
$Mo_2(O_2C\text{-}t\text{-}Bu)_4$	436	22950	100
	296	33800	10000
$W_2(O_2C\text{-}t\text{-}Bu)_4$	378	26450	19400
Mo_4(OXA)	500 sh	20000	8300
	460	21750	14200
	432 sh	23150	13100
	314 sh	31850	15800
	288	34700	17900
W_4(OXA)	704	14200	36400
	636	15700	28500
	582 sh	17200	16000
	368	27150	17200
Mo_4(PFT)	470	21300	10500
	322 sh	31050	11900
	288	34700	18000
W_4(PFT)	816	12250	27000
	354	28250	17300
Mo_4(DAND)	398	25150	13700
	320	31250	14600
	290	34500	16200
W_4(DAND)	552 sh	18100	20500
	510	19600	27800
	368	27150	21600
Mo_4(AND)	504	19850	10100
	394 sh	25400	8400
	370 sh	27050	12200
	358	27950	14200
	320 sh	31250	16400
	286	34950	21500
W_4(AND)	716	13950	18000
	470	21300	16800
	368	27150	27900
	348 sh	28750	24900
Mo_4(DOQ)	300	33350	26500
	314 sh	31850	24700
	328 sh	30500	20100
	440 sh	22750	9400
	474	21100	12200
	498 sh	20100	11200
Mo_4(DON)	438	22850	6800
	331 sh	32200	20500
	310	32250	26400
	294 sh	34050	24200

[a] All spectra recorded as solutions in THF.

of M_2 δ and ligand bridge π mixing whilst partially oxidized polymers should be conductive along the polymer chain.

Parallel-Linked M_4 Chains. The arrangement of an infinite chain of d^4 metal ions in a parallel mode should be subject to a Pierls distortion, i.e., we would anticipate alternating short and long M–M distances rather than the symmetric structure $(M{=}M{=}M{=}M)_\infty$. We have examined the bonding in parallel M_4 molecules by considering certain hypothetical and idealized geometries, again employing the Fenske–Hall calculational method.

When two $Mo_2H_8^{4-}$ units (Mo–Mo = 2.14 Å) are brought together to form a linear M_4 chain, the in-phase and out-of-phase Mo_2 δ combinations experience a splitting of only 0.57 eV at the relatively short "intermolecular" Mo–Mo distance of 2.40 Å. The calculated δ overlap integrals in the geometry $Mo_{(1)}\overset{2.14\text{ Å}}{-}Mo_{(2)}\overset{2.40\text{ Å}}{-}Mo_{(3)}\overset{2.14\text{ Å}}{-}Mo_{(4)}$ are $\langle d_{xy}(1)|d_{xy}(2)\rangle$ = 0.080 and $\langle d_{xy}(2)|d_{xy}(3)\rangle$ = 0.052. It is only at very short Mo–Mo distances (i.e., distances comparable to the Mo–Mo bond length) that we observe the development of a significant δ band.

We have also examined the bonding in a "slipped" M_4 chain consisting of two $M_2(O_2CH)_4$ units brought together such that "intermolecular" carboxylate oxygen to M bridge bonding can occur in a manner similar to that seen in the solid state, as shown in XII below. The relatively long M–O bond length of 2.67 Å provides a M–M separation of 3.08 Å. Not surprisingly, the calculations reveal a very small splitting of the in-phase and out-of-phase combinations of the M_2 δ orbitals, ca. 0.19 eV for M = W.

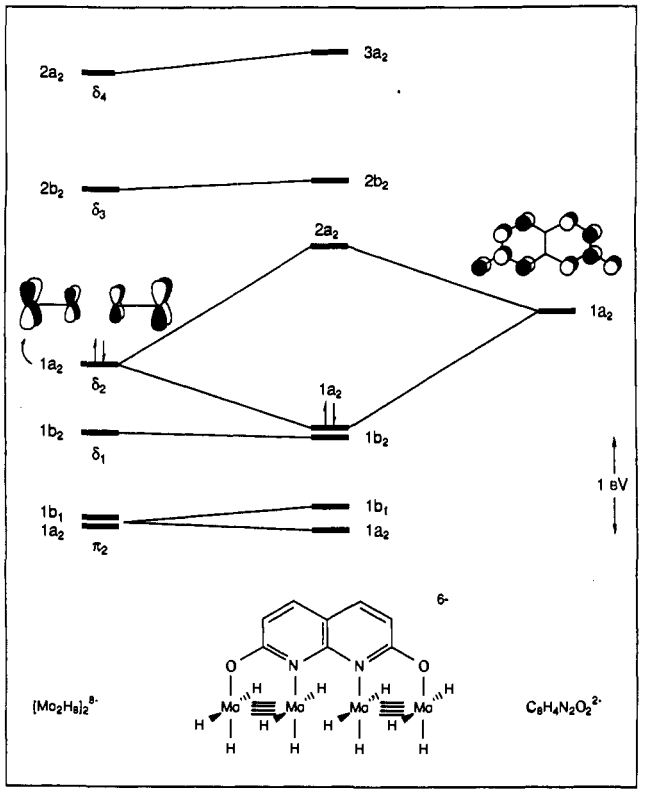

Figure 5. A frontier orbital interaction diagram showing the mixing of metal δ and naphthyridine π orbitals in the hypothetical compound $[Mo_2H_6]_2(\mu\text{-}2,7\text{-}O_2N_2C_8H_4)^{6-}$. The arrows denote the HOMO. Only the metal based HOMO and the 2,7-dioxynaphthyridine LUMO show a significant π interaction.

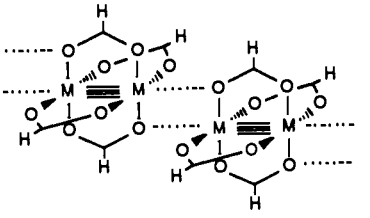

XII

In the case of the Mo_4(DON) complex the 2,7-dioxynaphthyridine bridge serves not only to orient the Mo atoms in a parallel manner but also to provide a conjugated π framework. We investigated the bonding in the model complex $[Mo_2H_6]_2(\mu\text{-}O_2N_2C_8H_4)^{6-}$ wherein the Mo_4 chain was constrained to be linear (C_{2v} symmetry). An interaction diagram depicting the frontier orbital region of the Mo_4 model complex is depicted in Figure 5. It is convenient first to construct the bonding picture of the Mo_4 chain in the absence of ligand π effects, as illustrated by $[Mo_2H_8]_2^{8-}$. As mentioned earlier, the two occupied Mo_4 δ combinations ($1b_2$ and $1a_2$ under C_{2v} symmetry) are split slightly in energy. The a_2 Mo_4 δ combination mixes extensively with the lowest energy empty π orbital of the dioxynaphthyridine ligand. The resulting interaction yields a lower energy HOMO and creates a ligand-based LUMO that contains significant metal character (40%). Therefore, like the perpendicular oxalate link, the dioxynaphthyridine ligand also provides an energetically favorable bridge for electronically coupling the two Mo_2 centers.

Electronic Spectra. In contrast to the light yellow quadruply bonded dinuclear starting materials, the dicarboxylate-linked tetranuclear compounds are more intensely colored and display a number of strong absorptions in the visible region of the elec-

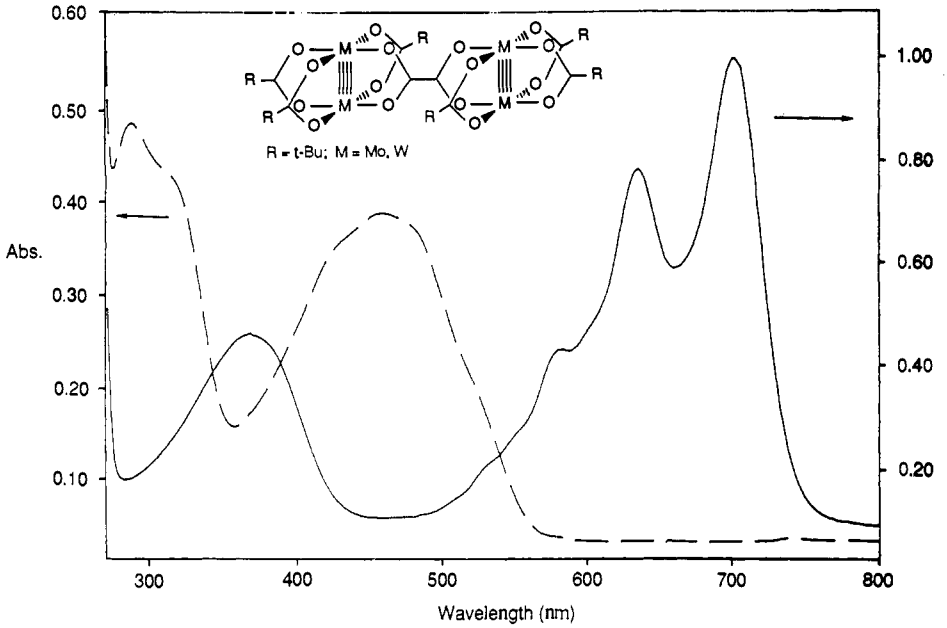

Figure 6. UV–visible spectra of M_4(OXA) compounds, where (--) = Mo and (—) = W, in tetrahydrofuran. The W_4(OXA) compound shows a strong red-shift relative to the Mo_4(OXA) compound as expected based on the frontier orbital energy diagram shown in Figure 3.

tronic spectrum. The energies and intensities of these absorptions are listed in Table IV for both the perpendicular- and parallel-linked molybdenum and tungsten M_4 species, along with the dinuclear starting materials for comparison. In the case of the M_2 compounds, the intense MLCT transitions are located in the ultraviolet region (M = Mo, 296 nm; M = W, 378 nm) and the only absorptions in the visible region are the weak $\delta \rightarrow \delta^*$ transitions (M = Mo, 436 nm; M = W, transition masked by MLCT band). The MLCT transitions for these $M_2(O_2CR)_4$ complexes have previously been assigned as M–M $\delta \rightarrow RCO_2$ π^* excitations.[20b,24] That the transition associated with the tungsten complex is 0.91 eV lower in energy, compared to the molybdenum complex, is consistent with the somewhat higher energy of tungsten 5d orbitals. The presence of MLCT transitions at significantly lower energies for the M_4 complexes indicates that the unsaturated dicarboxylate bridges provide vacant orbitals with energies lower than that of the corresponding ancillary carboxylate orbitals. Hence upon visible excitation charge transfer would take place from the metal centers to the dicarboxylate link.

The UV–vis spectra of the oxalate-bridged complexes, Mo_4(OXA) and W_4(OXA), are shown in Figure 6. The spectrum of the tungsten complex contains three intense, low-energy MLCT transitions, the strongest of which is centered at 704 nm. The energy and intensity of these transitions indicate that the LUMO must be the oxalate-based $3b_{2u}$ orbital. Under D_{2h} symmetry, excitation from the W–W δ-bonding HOMO ($3b_{3g}$) to the oxalate-based LUMO ($3b_{2u}$) is fully allowed (B_{1u}, Z polarized) and can be assigned to the band at 704 nm. Excitation from the lower energy W–W δ-bonding orbital ($2b_{2u}$) to the LUMO is forbidden as long as the molecule retains D_{2h} symmetry. Two of the W–W π-bonding combinations ($2b_{3g}$, $2a_g$) are of the appropriate symmetry to give rise to allowed transitions to the LUMO, and the bands at 636 and 582 nm are assigned to such excitations. The only other band observed for W_4(OXA) appears at 368 nm in the UV region and can be assigned to an excitation from the HOMO to a t-$BuCO_2$-based orbital. This transition parallels the MLCT transition observed for the simple dinuclear complex, with the only difference being that the excitation occurs at slightly shorter wavelength. This transition may in fact be a combination of two bands since the W_4 species contains two empty t-$BuCO_2$ π^* combinations, and excitations are symmetry-allowed from each of the W–W δ-bonding orbitals.

The electronic spectrum of Mo_4(OXA) is qualitatively similar to that of W_4(OXA). A set of three MLCT bands are located in the visible region, and two higher energy MLCT bands are found in the UV region. The three visible bands overlap considerably such that the absorptions are centered at 460 nm with a low-energy shoulder at 500 nm and a high-energy shoulder at 432 nm. These three bands are assigned to transitions from the Mo–Mo δ ($3b_{3g}$) and Mo–Mo π ($2b_{3g}$, $2a_g$) orbitals to the oxalate-based LUMO ($3b_{2u}$) from low to high energy, respectively. The energetic separations among these three bands are quite similar to that found for the same excitations in W_4(OXA). However, since the grouping is blue-shifted, and the wavelength separation is smaller, the bands overlap to a greater extent. It should be noted that the bands arising from transitions into the oxalate-based LUMO of Mo_4(OXA) are considerably less intense than the analogous transitions in W_4(OXA). This would be consistent with greater overlap between the W 5d orbitals and the oxalate π orbitals, thus allowing for a more facile charge transfer. The two bands found in the UV region are assigned as Mo–Mo δ to t-$BuCO_2$ transitions from both of the Mo–Mo δ combinations.

The electronic spectra of the perfluoroterephthalate-bridged complexes, Mo_4(PFT) and W_4(PFT), contain very broad MLCT bands in the visible region in addition to the bands associated with the t-$BuCO_2$ ligands found in the UV region. These broad bands are not as intense as the corresponding bands in the M_4(OXA) species and are centered at slightly lower energies. These transitions likely arise from excitation into closely spaced orbitals associated with the fluorinated aromatic ring of the dicarboxylate link. The electronegative fluorine substituents also act to lower the energy of these unoccupied orbitals.

The parallel-linked tetranuclear compounds bridged with either the 1,8-anthracenedicarboxylate or 9,10-dihydro-1,8-anthracenedicarboxylate ligands also display rich visible regions in their electronic spectra. Numerous studies concerning the electronic spectra of arylcarboxylate complexes of the type $M_2(O_2CAr)_4$ (M = Mo, W) have been undertaken, and their conclusions are particularly relevant here. Cotton et al. reported the presence of two MLCT bands for $W_2(O_2CPh)_4$, wherein the plane of the arene ring is aligned parallel to the plane of the carboxylate groups in the solid state but only a single band for $W_2(O_2C\text{-}C_6H_2(2,4,6\text{-}Me_3))_4$ in which the plane of the arene ring is forced to align perpendicular to the carboxylate group due to the steric bulk of the substituted ring.[19b] A similar effect was noted in the spectra of $W_2(O_2CPh)_4(np)_2$ and $W_2(O_2CC_6H_2(2,4,6\text{-}Me_3))_4(np)_2$ (np = neopentyl) by Chisholm et al.[25] The difference can be

(24) Santure, D. J.; Huffman, J. C.; Sattelberger, A. P. *Inorg. Chem.* **1985**, *24*, 371.

Scheme II

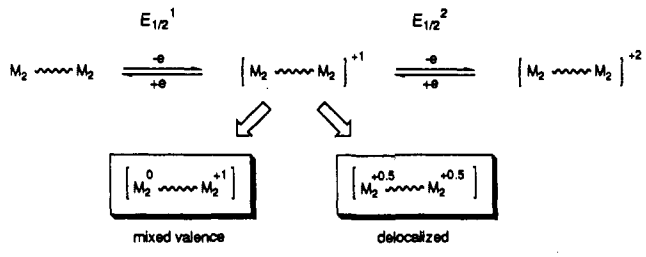

traced to a mixing of carboxylate π orbitals and arene π orbitals permitted only when the π sets are mutually parallel (conjugated), giving rise to two sets of allowed MLCT transitions. In the tetranuclear compounds, the anthracene backbone forces the arene rings to lie essentially parallel with the carboxylate groups, therefore the electronic picture may be expected to resemble more the unsubstituted benzoate M_2 species. The 9,10-dihydroanthracene backbone serves to separate electronically the two arene carboxylate functionalities and as such provides M_4(DAND) complexes whose spectra are indeed similar to the dinuclear benzoates. Two MLCT bands are found for both Mo_4(DAND) and W_4(DAND) along with the higher energy t-$BuCO_2$-based transitions. In the case of the fully conjugated anthracene-bridged complexes, Mo_4(AND) and W_4(AND), more complicated MLCT transitions are observed. This would be expected based on further mixing of carboxylate π orbitals with the arene π orbitals of three fused aromatic rings.

Electrochemistry. The electrochemical properties of the dinuclear $M_2(O_2CR)_4$ (M = Mo, W) complexes containing M–M quadruple bonds have been extensively investigated.[24-26] In general, these complexes exhibit two oxidation processes as determined by cyclic voltammetry. The first oxidation process is quasi-reversible, while the second oxidation is essentially irreversible (at scan rates on the order of 100 mV/s). The redox couple occurring at lower potentials has been shown by coulometry to be a one-electron process, the potential of which is greatly influenced by the nature of both the carboxylate ligands and the metal centers. For example, the oxidation potential is generally lowered in the case of good electron-donating carboxylates and for M = W compared to M = Mo. The oxidation process has been assigned to the removal of an electron from the primarily M–M δ-bonding orbital. This is consistent with the more facile oxidation of the ditungsten complexes since their metal-based orbitals are ca. 0.5–1.0 eV higher in energy than the corresponding molybdenum-based orbitals. In addition, the paramagnetic one-electron-oxidized complexes, $M_2(O_2CR)_4^{1+}$, are in certain cases isolable and have been prepared by chemical oxidation for M = Mo[27] and W[24] as well as for the mixed-metal species, $MoW(O_2C$-t-$Bu)_4^{1+}$.[28] These cationic compounds contain a formal M–M bond order of 3.5.

We were interested in studying the electrochemistry of the covalently linked M_4 complexes reported here in order to assess the influence of the various unsaturated bridges, and their respective geometrical constraints, upon the redox behavior of the coupled dinuclear centers. Concentrating on the initial oxidation process of each multiple bond, there are two limiting scenarios that may be realized, as depicted in Scheme II. The symbol M_2 represents a dimolybdenum or ditungsten quadruply bonded unit and --- represents the bridging link. Scheme II depicts the oxidation of two neutral linked quadruple bonds to a tetranuclear dication via two discrete steps, with corresponding redox potentials,

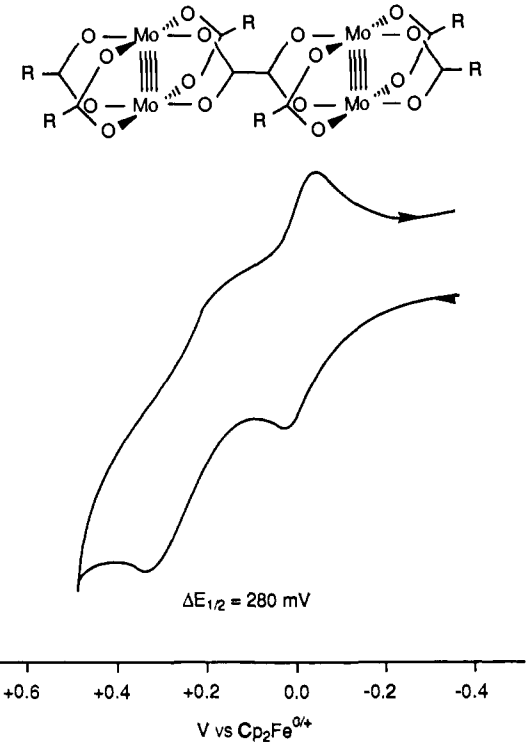

Figure 7. Cyclic voltammogram of Mo_4(OXA) showing the $Mo_4(OXA)^{0/1+}$ and $Mo_4(OXA)^{1+/2+}$ redox processes. The first couple is reversible, and the second is not.

$E_{1/2}^1$ and $E_{1/2}^2$. The difference between the two redox potentials ($\Delta E_{1/2}$) will vary significantly depending upon the nature of the monocationic intermediate. If the bridging ligand behaves as an insulator (i.e. provides no facile means for electron transfer between the redox active sites), the electronic communication between the isolated M_2 centers will be small, and the monocation intermediate will exhibit a mixed-valence ground state. In this case the difference in potential between the $E_{1/2}$ values will be small ($\Delta E_{1/2}$ = 35.6 mV in the limit of no interaction) and the current-potential response will have the same shape as that exhibited by a single one-electron center.[29] On the other extreme, if electron transfer is sufficiently rapid through the bridging ligand the positive charge will be delocalized over all four metal atoms in the intermediate monocation. In this case the second oxidation step should occur at a much higher potential than the first, and thus result in a large $\Delta E_{1/2}$. Cyclic voltammetry and differential pulse voltammetry are convenient methods for determining the $E_{1/2}$ values of these stepwise oxidation–reduction couples, which in turn can be used to determine the stability of the tetranuclear monocationic intermediate with respect to disproportionation to neutral and dicationic species as shown in eq 7.[30] As written,

$$[M_2\text{---}M_2] + [M_2\text{---}M_2]^{2+} \overset{K_c}{\rightleftharpoons} 2[M_2\text{---}M_2]^{1+} \qquad (7)$$

$$K_c = \exp(\Delta E_{1/2}/25.69)$$

K_c represents a comproportionation equilibrium constant whose magnitude is directly proportional to the difference in successive redox potentials. Therefore, the greater the degree of delocalization in the monocation, the greater the difference in successive oxidation potentials, hence the larger the value of K_c, and the more stable the monocation. It should be noted that even completely noninteracting metal centers would yield a K_c = 4. The system is analogous to that studied by Taube and co-workers for mononuclear complexes, e.g., $Ru^{II/III}$-bridged-$Ru^{II/III}$ systems.[31] A

(25) Chisholm, M. H.; Clark, D. L.; Huffman, J. C.; van der Sluys, W. G.; Kober, E. M.; Lichtenberger, D. L.; Bursten, B. E. *J. Am. Chem. Soc.* **1987**, *109*, 6796.
(26) (a) Cotton, F. A.; Pedersen, E. *Inorg. Chem.* **1975**, *14*, 399. (b) Zietlow, T. C.; Klendworth, D. D.; Ninry, T.; Salmon, D. J.; Walton, R. A. *Inorg. Chem.* **1981**, *20*, 947.
(27) McCarley, R. E.; Templeton, J. L.; Colburn, T. J.; Katovic, V.; Hoxmeier, R. J. *Adv. Chem. Ser.* **1976**, *150*, 318.
(28) Katovic, V.; Templeton, J. L.; Hoxmeier, R. J.; McCarley, R. F. *J. Am. Chem. Soc.* **1975**, *97*, 5300.
(29) (a) Ammar, F.; Saveant, J. M. *J. Electroanal. Chem.* **1973**, *47*, 215. (b) Flanagan, J. B.; Margel, S.; Bard, A. J.; Anson, F. C. *J. Am. Chem. Soc.* **1978**, *100*, 4248.
(30) Richardson, D. E.; Taube, H. *Inorg. Chem.* **1981**, *20*, 1278.
(31) Taube, H. *Angew. Chem., Int. Ed. Engl.* **1984**, *23*, 329, and references therein.

Table V. Electrochemical Data for the Series of Linked Tetranuclear Complexes, $[M_2(O_2C\text{-}t\text{-}Bu)_3]_2$(bridge), Along with the Dinuclear Compounds, $M_2(O_2C\text{-}t\text{-}Bu)_4$ (M = Mo, W)

compound[a]	$E_{1/2}{}^1$ [b](V)	ΔE_p [c](mV)	$E_{1/2}{}^2$ (V)	ΔE_p (mV)	$\Delta E_{1/2}$ [d](mV)	K_c[e]
$Mo_2(O_2C\text{-}t\text{-}Bu)_4$	−0.04	78				
$W_2(O_2C\text{-}t\text{-}Bu)_4$	−0.70	98				
Mo_4(OXA)	−0.03	79	+0.25	110	280	5.4×10^4
W_4(OXA)	−1.26	105	−0.54	161	717	1.3×10^{12}
Mo_4(PFT)	+0.10[f]	92			65	13
W_4(PFT)	−0.66	70	−0.37	183	285	6.6×10^4
W_4(FDC)	−0.81	97	−0.72	94	93	37
Mo_4(DOQ)	−0.13	144	+0.26	209	391	4.1×10^6
DPV[g]	−0.13		+0.24		366	1.5×10^6
Mo_4(DAND)	−0.03	74	+0.08	752	106	62
W_4(DAND)	−0.70	89	−0.55	79	146	2.9×10^2
W_4(AND)	−0.66	75	−0.51	77	156	4.3×10^2
Mo_4(DON)	−0.07	83	+0.32	162	389	3.8×10^6
DPV[g]	−0.08		+0.30		373	2.0×10^6

[a] All compounds were studied as 1×10^{-3} M solutions in THF containing 0.2 M $(n\text{-}Bu)_4NPF_6$ as the supporting electrolyte. The potentials were determined by cyclic voltammetry at a scan rate of 100 mV/s unless otherwise specified and are referenced to the $Cp_2Fe^{0/+}$ couple used as an internal reference (+0.89 V vs the Ag wire pseudoreference, ΔE_p = 70 mV). [b] $E_{1/2}$ = half wave potential of redox couple. [c] ΔE_p = difference between anodic and cathodic peak potentials. [d] $\Delta E_{1/2}$ = difference between successive redox couples, i.e., $\Delta E_{1/2} = E_{1/2}{}^2 - E_{1/2}{}^1$. [e] K_c = comproportionation equilibrium constant. [f] The potential represents the average $E_{1/2}$ value for both redox couples involving the removal of two electrons. [g] Data obtained by differential pulse voltammetry (rate = 5 mV/s, pulse amplitude = 25 mV) for Mo_4(DON).

K_c value of greater than 10^6 implies extensive, if not complete, delocalization of charge between the metal centers, class III on the Robin and Day scheme,[32] while a K_c value of 100 or less corresponds to little delocalization or a valence-trapped system, class I. With intermediate K_c values for 10^2 to 10^6 then an intermediate degree of delocalization is attained, so called class II behavior. The redox potentials of all the tetranuclear complexes were determined by cyclic voltammetry, and the results are presented in Table V, along with the half potentials of the parent dinuclear complexes.

Perpendicular-Linked M_4 Complexes. A representative cyclic voltammogram of Mo_4(OXA) is shown in Figure 7. The scan indicates the presence of two distinct redox couples, the first of which appears to be quasi-reversible based on the ratio of anodic to cathodic current flow (i_{pa}/i_{pc} = 1.1), whereas the second couple is essentially irreversible. By comparing the magnitude of the current flow for each oxidation wave of Mo_4(OXA) with that of an equimolar solution of $Mo_2(O_2C\text{-}t\text{-}Bu)_4$ under identical conditions (wherein $Mo_2(O_2C\text{-}t\text{-}Bu)_4$ is known to undergo a one-electron oxidation) both oxidations were found to be one-electron processes.

The first oxidation of Mo_4(OXA) occurs at a potential very similar to that of the dinuclear compound $Mo_2(O_2C\text{-}t\text{-}Bu)_4$ (cf. −0.03 V for Mo_4 and −0.04 V for Mo_2 vs $Cp_2Fe^{0/+}$); however, the second oxidation occurs 280 mV higher in potential. This corresponds to a K_c of 5.4×10^4 and indicates that electron transfer through the oxalate ligand is allowing the two Mo_2 quadruply bonded centers to be in "communication" in the one-electron-oxidized species. According to the classification of Robin and Day[32] for mixed-valence systems, the cation $Mo_4(OXA)^+$ could be considered as a class II species.

The cyclic voltammogram of W_4(OXA) is depicted in Figure 8, and, when compared to that of Mo_4(OXA), some interesting similarities and differences surface. As before, two oxidation waves are observed, each involving only one electron. The first couple displays quasireversible behavior, while the second oxidation wave appears to be essentially irreversible upon the reduction sweep. One significant difference in the CV of the oxalate-bridged tungsten complex lies in the $W_4(OXA) \rightleftarrows W_4(OXA)^+$ couple: the initial oxidation occurs at −1.26 V which is 0.56 V lower in potential than the first oxidation of the parent dinuclear complex $W_2(O_2C\text{-}t\text{-}Bu)_4$. In general, quadruply bonded ditungsten complexes exhibit oxidation potentials ca. 0.7 V lower than isoelectronic dimolybdenum complexes (cf. $M_2(O_2C\text{-}t\text{-}Bu)_4$; $E_{1/2}$ = −0.70 V (M = W), −0.04 V (M = Mo), see Table V) due to the higher energy of W 5d orbitals. However, in this case $E_{1/2}{}^1$ of W_4(OXA) is found to be 1.23 V lower than the corresponding $E_{1/2}{}^1$ of

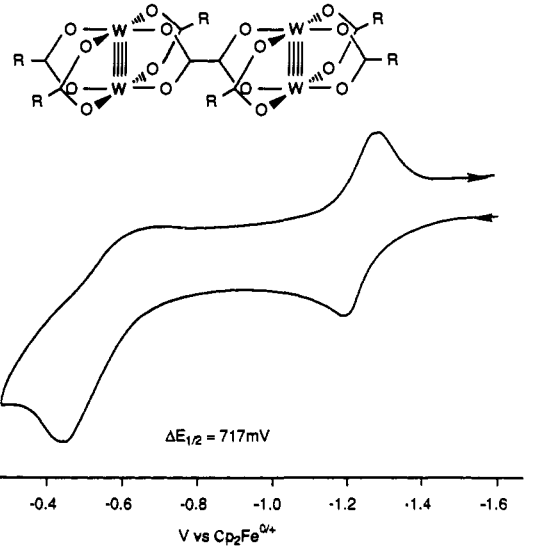

Figure 8. Cyclic voltammogram of W_4(OXA) showing the 0/1+ and 1+/2+ redox processes and the much greater separation between couples compared to the molybdenum analogue shown in Figure 7.

Mo_4(OXA). Furthermore, the separation between the successive redox processes of W_4(OXA) is substantially greater at 717 mV than that of Mo_4(OXA). This results in a K_c of 1.3×10^{12} and indicates that the cation $W_4(OXA)^+$ does not exist as a charge-separated mixed-valence species but rather exhibits a delocalized ground state involving the oxalate π system wherein electron transfer is rapid, class III behavior.

Compared to the oxalate link, the perfluorinated terephthalate ligand (1,4-$(O_2C)_2C_6F_4$) represents a somewhat longer bridging group, yet retains a conjugated π system. The effect this longer bridge has upon the oxidation behavior of the resulting compounds, Mo_4(PFT) and W_4(PFT), is as one might expect; electronic communication is not as great, and the successive redox processes are not as widely separated (see Table V). In fact, in the case of Mo_4(PFT) the two redox couples are so close in potential that the cyclic voltammogram cannot resolve separate oxidation waves, and the net result is a single wave representing the summation of two closely spaced redox couples. The observed E_{pa} and E_{pc} values for the combined curves does not vary significantly with scan rate, and from the peak separation (ΔE_p = 92 mV) a value for $\Delta E_{1/2}$ can be estimated at 65 mV based upon the method of Taube and Richardson.[30] This yields a K_c of only 13 for $Mo_4(PFT)^+$ indicating that the cation is a mixed-valence, class I species. As with the oxalate system, the perfluoroterephthalate-bridged tungsten compound displays stronger coupling

(32) Robin, M. B.; Day, P. *Adv. Inorg. Chem. Radiochem.* **1967**, *10*, 247.

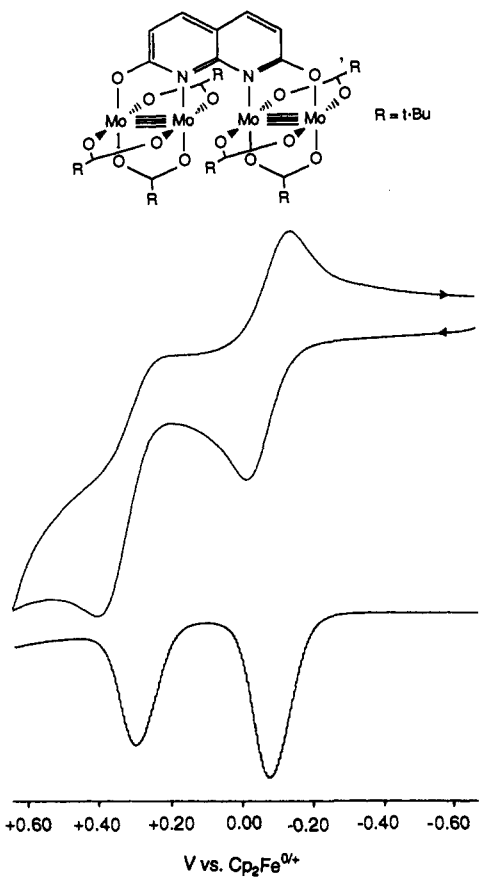

Figure 9. A comparison of the cyclic voltammogram and differential pulse voltammogram for the 2,7-dioxynaphthyridine complex Mo_4(DON) depicting the 0/1+ and 1+/2+ redox processes. The first couple is reversible, the second is not.

Table VI. A Summary of Crystal Data for Mo_4(DON)

empirical formula	$C_{54}H_{74}Mo_4N_2O_{18}$
color of crystal	orange
crystal dimensions (mm)	0.25 × 0.25 × 0.25
space group	$P\bar{1}$
cell dimensions	
temp °C	−169
a (Å)	15.714 (3)
b (Å)	14.923 (2)
c (Å)	15.109 (2)
α (deg)	113.37 (1)
β (deg)	104.50 (1)
γ (deg)	66.51 (1)
Z (molecules/cell)	2
volume (Å^3)	3163.34
calculated density (gm/cm^3)	1.494
wavelength (Å)	0.71069
molecular weight	1422.94
linear absorption coeff (cm^{-1})	8.193
detector-to-sample distance (cm)	22.5
sample-to-source distance (cm)	23.5
av ω scan width at half height	.25
scan speed (deg/min)	8.0
scan width (deg + dispersion)	1.8
individual background (s)	4
aperture size (mm)	3.0 × 4.0
2θ range (deg)	6–45
total number of reflcns collected	10939
no. of unique intensities	8275
no. with $F > 0.0$	7541
no. with $F > 3.0\sigma(F)$	6656
$R(F)$	0.0612
$Rw(F)$	0.0641
goodness of fit for the last cycle	1.494
max δ/σ for last cycle	0.055

than its molybdenum analogue. For W_4(PFT) the two redox waves are separated by 285 mV ($K_c = 6.6 \times 10^4$). The striking difference in the oxidation behavior of W_4(OXA) and W_4(PFT) lies in the potential of the initial oxidation. Whereas W_4(OXA) is oxidized 0.56 V *lower* in potential than $W_2(O_2C\text{-}t\text{-}Bu)_4$, W_4(PFT) exhibits its first oxidation 0.04 V *higher* in potential.

The redox chemistry of the 1,1′-ferrocenedicarboxylate-bridged compound is interesting because of the number of potentially redox-active centers. In isolation, we would expect the W_2 centers to be more readily oxidized than the Cp_2Fe fragment, and indeed the system seems to behave as expected. The successive redox couples are observed at negative potentials with respect to $Cp_2Fe^{0/+}$ and are separated by 90 mV, indicating that the oxidation processes likely involve the W_2 centers and only a small degree of electronic communication is operative. Presumably the small degree of electronic communication reflects the lack of carboxylate CO_2–cyclopentadienyl conjugation. However, even with CO_2–C_5H_4 conjugation the W_2-to-W_2 distance could well be long enough to preclude significant coupling.

The 2,3-dioxyquinoxaline bridge of the compound Mo_4(DOQ) is stereochemically correspondent to the oxalate bridge of Mo_4(OXA), but the electrochemical data indicate that the two Mo_2 centers are more strongly coupled: $\Delta E_{1/2} = 366$ mV ($K_c = 1.5 \times 10^6$) for Mo_4(DOQ) versus $\Delta E_{1/2} = 280$ mV ($K_c = 5.4 \times 10^4$) for Mo_4(OXA).

Parallel-Linked Dicarboxylate-Bridged M_4 Complexes. Electron transfer between the dimetal centers in the perpendicular-linked model complexes is constrained to take place *through* the dicarboxylate bridge since the metal centers are positioned too far apart for any direct orbital overlap (in the shorter oxalate-linked system the two M_2 units are separated by ca. 7.0 Å). By contrast,

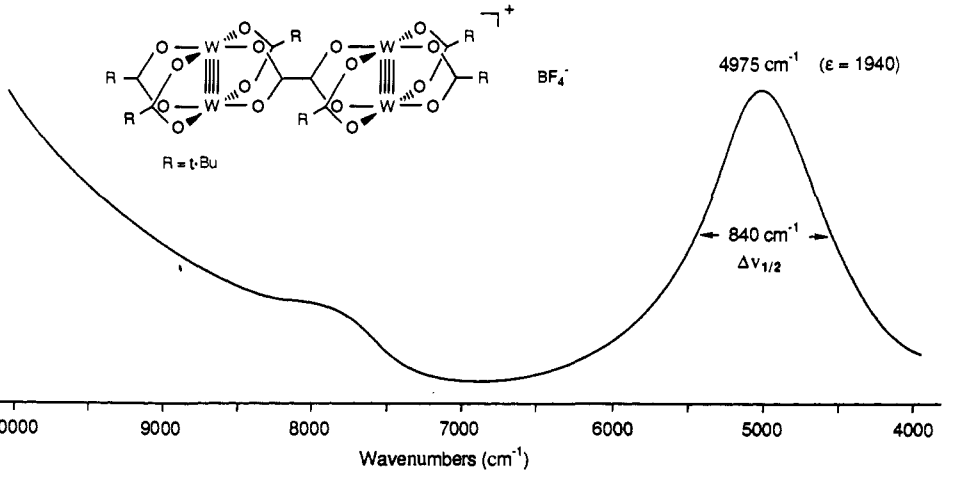

Figure 10. Near-IR spectrum of the one-electron-oxidized tetranuclear complex, $W_4(OXA)^+BF_4^-$, in tetrahydrofuran.

in the parallel model systems [M_4(AND), M_4(DAND), and Mo_4(DON)] two potential electron-transfer pathways are available: (1) via the ligand bridge in a manner similar to the perpendicular compounds or (2) via direct metal–metal interaction which is now facilitated by the proximity of the M_2 units induced by the rigid span. The preferred pathway can be determined by a comparison of the electrochemical results. Saturation of the central aromatic anthracene ring serves to disrupt the π conjugation and would therefore impede through-bridge electron transfer. However, saturation does not greatly affect the geometry of the M_4 core and as such would not be expected to significantly alter a pathway based on direct metal–metal interaction. For the saturated derivatives, M_4(DAND), two separate redox couples can be distinguished for both M = Mo and W with $\Delta E_{1/2}$ values of 106 and 146 mV, respectively. In both cases the electronic coupling is relatively weak and the one-electron-oxidized monocations are best described as mixed-valence species: K_c = 62 (Mo) and 290 (W). As before the W_4 complex displays stronger coupling than the Mo_4 analogue. In the case of the 1,8-anthracenedicarboxylate bridged compounds only the oxidation of the W_4 complex can be studied because initial oxidation of the Mo_4 complex occurs from the anthracene ligand. The $\Delta E_{1/2}$ value for W_4(AND) is 156 mV which differs little from W_4(DAND). Two points are worthy of note: (i) the relative weak coupling between the two M_2 centers and (ii) the small difference between the saturated and unsaturated ligand-bridged complexes. This suggests a situation involving poor, direct M_2–M_2 electron transfer as might have been anticipated based on the results of the calculations presented earlier.

By contrast, the 2,7-dioxynaphthyridine-bridged Mo_4 complex, which is stereochemically similar to the M_4(AND) complexes, shows very strong coupling as evidenced by the $\Delta E_{1/2}$ = 373 mV and $K_c = 2.0 \times 10^6$ determined from cyclic voltammetry and differential pulsed voltammetry, see Figure 9. This indicates that in Mo_4(DON) the electronic communication is via the ligand bridge as too might have been anticipated based on our earlier discussion of the calculations.

M_4-Bridged Radical Cations. The neutral M_4-bridged compounds may be chemically oxidized, and we have isolated some examples than span the range of valence-trapped, class I, to delocalized, class III systems. See eq 5. These salts are paramagnetic; they show axial ESR parameters, and the signals are quite broad. No superhyperfine interactions involving Mo and W spin active nuclei were resolved. The UV–visible spectra were very similar to those of the neutral M_4-bridged complexes, and only in one instance did we clearly observe a low-energy, near-IR absorption, namely in the case of $W_4(OXA)^+BF_4^-$. The latter is shown in Figure 10. The absorption of λ_{max} ca. 5000 cm^{-1} has $\epsilon \sim 2000$ and a width at half height of ca. 800 cm^{-1}. Compared to typical intervalence CT bands this is quite sharp and intense and is relatively solvent or medium insensitive.[22f] This is consistent with a delocalized ground state for the $W_4(OXA)^+$ radical cation.

Concluding Remarks

We have prepared the first series of covalently linked M–M quadruply bonded tetranuclear complexes and have shown that by suitable ligand selection the alignment of the M_2 units can be in either a parallel or perpendicular mode. The electronic coupling between the M_2 centers is extremely sensitive to the ligand bridge and the metal (M = Mo versus W). Many similarities are seen with ligand-bridged dinuclear systems of the type studied by Taube and his co-workers. In the latter instance it was shown that the coupling derives from metal $t_{2g}^6(d_\pi)$–ligand π orbital mixing and is sensitive to the orbital energies of the metal.[33] For example, for π acid ligands the coupling is greater for osmium relative to ruthenium. Moreover, as the length of the conjugated π bridge increases the coupling decreases. A similar situation is now seen for the M_4 systems wherein the M_2 δ and ligand π orbitals mix and the K_c values for M = W are much greater than for M = Mo. Despite the close M_2–M_2 separations in the parallel-linked M_4 complexes the electronic coupling is weak unless the ligand bridge intercedes as is the case for the 2,7-dioxynaphthyridine-bridged complex.

Particularly encouraging to us are the calculations employing the Fenske–Hall method on model M_4 systems. These, though qualitative, assist in understanding both the electronic spectra and the origin of the electronic coupling between the M_2 centers. The calculations identify the key orbital interactions and furthermore lead to an anticipation of the electronic properties of polymer chains built up from covalently linked M_2 subunits.

The stability of the M_4 compounds reported here also impacts on the likely stability of the corresponding polymers. Only for certain bridging groups do we find that ligand scrambling is not facile. Thus kinetic persistence of a polymer chain in solution will probably be limited to these and related bridging ligands. The selection of ligand bridge may also be expected to yield polymers having semiconducting or metallic properties irrespective of the mode of linkage. However, while the parallel alignment of Mo_2 units does not lend itself to orbital mixing in absence of a suitable bridge, the related M_4 complex involving Ru^{II}–Ru^{II} subunits might be expected to show strong metal orbital mixing because of the M–M valence configuration $\sigma^2\pi^4\delta^2\delta^{*2}\pi^{*2}$. These matters remain the subject of future work and consideration.

Experimental Section

Physical Techniques. ^{1}H NMR spectra were recorded on a Varian XL300 spectrometer at 300 MHz in dry and oxygen-free pyridine-d_5, dimethyl sulfoxide-d_6, or acetone-d_6. ^{19}F NMR spectra were recorded on a Nicolet NT-360 spectrometer at 340 MHz in acetone-d_6. All ^{1}H NMR chemical shifts are reported in ppm relative to the protio impurity resonances as follows: pyridine-d_5, singlet at 7.19 ppm; dimethyl sulfoxide-d_5, quintet at 2.49 ppm; acetone-d_6, quintet at 2.04 ppm; acetonitrile-d_3, quintet at 1.93 ppm; and methylene chloride-d_2, triplet at 5.32 ppm. The ^{19}F NMR chemical shifts are reported in ppm relative to $CFCl_3$ at 0.00 ppm.

Infrared spectra were recorded on a Nicolet 510P FT-IR spectrophotometer as KBr pellets in the region covering 4000 to 400 cm^{-1}.

Ultraviolet and visible absorption spectra were recorded on a Hewlett Packard 8452A diode array spectrophotometer with a 1.00-cm quartz cell. All spectra were recorded in dry and oxygen-free tetrahydrofuran from which a spectrum of the neat solvent in the same cell was subtracted. The extinction coefficients reported were reproducible to ±10%.

Near-infrared spectra were recorded on a Perkin-Elmer Lambda 9 spectrophotometer with a 1.00-cm infrasil cell in the region 12 500 to 4500 cm^{-1} and on a Nicolet 510P FT-IR spectrophotometer with a 0.1-mm KBr cell in the region 7200 to 4000 cm^{-1}.

Electrochemical measurements were obtained with a PAR 173 potentiostat and 175 programmer along with a Houston Instruments 2000 XY recorder. The cyclic voltammograms were recorded either in a Vacuum Atmospheres drybox or in an airless cell under an N_2 atmosphere. In all cases the solvent used was tetrahydrofuran, 2.0 M in tetra-*n*-butylammonium hexafluorophosphate as the supporting electrolyte. The working electrode was a platinum wire encased in a cobalt-tipped electrode. The counter electrode was a platinum-gauze electrode. A silver wire was used as pseudoreference electrode. All potentials reported are relative to the $(C_5H_5)_2Fe/(C_5H_5)_2Fe^+$ couple which occurs at +0.89 V (ΔE_p = 70 mV) under the conditions specified above.

Elemental analyses were performed by Oneida Research Services, Whitesboro, NY, and all compounds were handled with inert atmosphere techniques.

Synthesis. All reactions were carried out under an atmosphere of dry and oxygen-free nitrogen with standard Schlenk and glovebox techniques. All solvents were dried and degassed by standard methods and distilled prior to use. Oxalic acid (anhydrous), perfluoroterephthalic acid, 1,1′-ferrocenedicarboxylic acid, 2,3-dihydroxyqunioxaline, trimethyloxonium tetrafluoroborate, triethyoxonium tetrafluoroborate (1.0 M in CH_2Cl_2), *n*-butyllithium (1.6 M in hexane), sodium methoxide (4.4 M in methanol), and silver hexafluorophosphate were purchased from Aldrich and used as received. Dimolybdenum tetrapivalate,[34] ditungsten tetrapivalate,[35] anthracene-1,8-dicarboxylic acid,[36] 9,10-dihydroanthracene-

(33) Richardson, D. E.; Sen, J. P.; Buhr, J. D.; Taube, H. *Inorg. Chem.* **1982**, *21*, 3136.

(34) Brignole, A. G.; Cotton, F. A. *Inorg. Synth.* **1972**, *13*, 81.

(35) Santure, D. J.; Huffman, J. C.; Sattelberger, A. P. *Inorg. Chem.* **1985**, *24*, 371.

1,8-dicarboxylic acid,[36] and 2,7-dihydroxynaphthyridine[37] were prepared by published procedures.

$[Mo_2(O_2C\text{-}t\text{-}Bu)_3]_2(O_2C\text{-}CO_2)$, Mo_4(OXA). To a flask containing 1.000 g (1.68 mmol) of $Mo_2(O_2C\text{-}t\text{-}Bu)_4$ and 0.0755 g (0.84 mmol) of anhydrous oxalic acid was added 20 mL of toluene. The reaction was stirred at room temperature for 3 days. Over this time the yellow reaction mixture turned red and a red powder fell out of solution. The reaction mixture was filtered through a fine frit, and the solid was washed with 3 × 20 mL of toluene and 3 × 25 mL of hexane and then dried under vacuum to yield 0.859 g (95%) of analytically pure red powder. The compound can be crystallized from concentrated pyridine solutions at −20 °C to yield red needles that retain 0.7 pyridine molecules per Mo_2 unit based on ^{1}H NMR and elemental analysis: ^{1}H NMR (22 °C) pyridine-d_5 δ 1.55 (s, 36 H), 1.56 (s, 18 H); dimethylsulfoxide-d_6 δ 1.38 (s, 36 H), 1.39 (s, 18 H); IR (cm^{-1}) 2963 (m), 1543 (s), 1485 (vs), 1460 (m), 1420 (s), 1379 (m), 1366 (m), 1302 (m), 1225 (ms), 899 (mw), 777 (m), 617 (m).

Anal. Calcd for $C_{32}H_{54}O_{16}Mo_4 \cdot 1.4(C_5H_5N)$: C, 39.39; H, 5.17; N, 1.65. Found: C, 39.41; H, 4.86; N, 1.63.

$[Mo_2(O_2C\text{-}t\text{-}Bu)_3]_2(O_2C\text{-}1,4\text{-}C_6F_4\text{-}CO_2)$, Mo_4(PFT). To a flask containing 0.400 g (0.67 mmol) of $Mo_2(O_2C\text{-}t\text{-}Bu)_4$ and 0.0878 g (0.37 mmol) of tetrafluoroterephthalic acid was added 15 mL of toluene. The reaction was stirred at room temperature for 4 days over which time the yellow color changed to yellow-orange and a precipitate appeared. The precipitate was collected by filtration through a fine frit, washed with 2 × 20 mL of toluene followed by 3 × 10 mL of hexane, and then dried under vacuum to yield 0.380 g (92%) of light orange analytically pure material: ^{1}H NMR (22 °C), pyridine-d_5 δ 1.58 (s, 18 H), 1.64 (s, 36 H); acetone-d_6 1.42 (s, 18 H), 1.45 (s, 36 H); ^{19}F NMR (22 °C), acetone-d_6 δ −140.41 (s); IR (cm^{-1}) 2963 (m), 1534 (s), 1485 (vs), 1420 (s), 1399 (ms), 1379 (m), 1366 (m), 1223 (m), 990 (m), 897 (w), 748 (m), 617 (m). Anal. Calcd for $C_{38}H_{54}F_4O_{16}Mo_4$: C, 37.21; H, 4.44; F, 6.20. Found: C, 37.17; H, 3.93; F, 8.21.

$[Mo_2(O_2C\text{-}t\text{-}Bu)_3]_2(O_2C\text{-}1,8\text{-}C_{14}H_8\text{-}CO_2)$, Mo_4(AND). To a flask containing 2.000 g (3.35 mmol) of $Mo_2(O_2C\text{-}t\text{-}Bu)_4$ and 0.4911 g (1.84 mmol) of anthracene-1,8-dicarboxylic acid was added 30 mL of toluene. The reaction was stirred at room temperature for 3 days to give an orange precipitate and nearly colorless solution. The mixture was filtered through a fine frit, and the solid was washed with 3 × 15 mL of toluene followed by 3 × 10 mL of hexane and then dried under vacuum to yield 1.933 g (92%) of orange solid. The compound was purified by crystallization from a concentrated pyridine solution at −20 °C: ^{1}H NMR (22 °C) pyridine-d_5 δ 1.49 (s, 36 H), 1.65 (s, 18 H), 7.42 (dd, $^3J_{HH}$ = 7 Hz, 9 Hz, 2 H), 8.08 (d, $^3J_{HH}$ = 9 Hz, 2 H), 8.48 (s, 1 H), 8.61 (dd, $^3J_{HH}$ = 7 Hz, $^4J_{HH}$ = 1 Hz, 2 H), 12.81 (s, 1 H); variable-temperature ^{1}H NMR, THF-d_8 +20 °C δ 1.30 (s, 36 H), 1.46 (s, 18 H), 7.61 (dd, $^3J_{HH}$ = 7 Hz, 8 Hz, 2 H), 8.20 (d, $^3J_{HH}$ = 9 Hz, 2 H), 8.44 (dd, $^3J_{HH}$ = 7 Hz, $^4J_{HH}$ = 2 Hz, 2 H), 8.60 (s, 1 H), 12.00 (s, 1 H); −100 °C δ 1.11 (s, 18 H), 1.43 (s, 18 H), 1.45 (s, 18 H), 7.73 (t, 2 H), 8.36 (d, 2 H), 8.50 (d, 2 H), 8.75 (s, 1 H), 11.87 (s, 1 H); $\Delta G^{\ddagger}$ (−80 °C) = 9.1 kcal/mol; IR (cm^{-1}) 2963 (m), 1487 (vs), 1420 (s), 1401 (m), 1379 (m), 1366 (mw), 1221 (m), 897 (w), 617 (m). Anal. Calcd for $C_{46}H_{62}O_{16}Mo_4$: C, 44.03; H, 4.98. Found: C, 43.71; H, 4.53.

$[Mo_2(O_2C\text{-}t\text{-}Bu)_3]_2(O_2C\text{-}1,8\text{-}C_{14}H_{10}\text{-}CO_2)$, Mo_4(DAND). To a flask containing 0.300 g (0.50 mmol) of $Mo_2(O_2C\text{-}t\text{-}Bu)_4$ and 0.0742 g (0.28 mmol) of 9,10-dihydroanthracene-1,8-dicarboxylic acid was added 8 mL of toluene. The reaction was stirred at room temperature for 3 days over which time a fine yellow powder fell out of the solution. The yellow solid was collected by filtration through a fine frit, washed with 2 × 10 mL of toluene (in which the solid appeared to be slightly soluble) followed by 2 × 10 mL of hexane, and then dried under vacuum to yield 0.187 g (59%) of analytically pure material: ^{1}H NMR (22 °C) pyridine-d_5 δ 1.52 (s, 36 H), 1.62 (s, 18 H), 3.83 (s, 2 H), 5.89 (s, 2 H), 7.19 (t, $^3J_{HH}$ = 7 Hz, 2 H), 7.29 (d, $^3J_{HH}$ = 7 Hz, 2 H), 8.31 (d, $^3J_{HH}$ = 7 Hz, 2 H); variable-temperature ^{1}H NMR, THF-d_8 +20 °C δ 1.32 (s, 36 H), 1.43 (s, 18 H), 4.09 (s, 2 H), 5.55 (s, 2 H), 7.27 (t, $^3J_{HH}$ = 7 Hz, 2 H), 7.43 (d, $^3J_{HH}$ = 7 Hz), 8.05 (d, $^3J_{HH}$ = 7 Hz); −100 °C δ 1.17 (s, 18 H), 1.41 (s, 18 H), 1.42 (s, 18 H), 4.09 (s, 2 H), 5.48 (s, 1 H), 7.35 (t, 2 H), 7.54 (d, 2 H), 8.04 (d, 2 H); $\Delta G^{\ddagger}$ (−80 °C) = 9.1 kcal/mol; IR (cm^{-1}) 2961 (m), 1487 (vs), 1420 (s), 1379 (m), 1366 (mw), 1262 (w), 1221 (m), 897 (w), 617 (m). Anal. Calcd for $C_{46}H_{64}O_{16}Mo_4$: C, 43.96; H, 5.13. Found: C, 45.07; H, 4.77.

$[W_2(O_2C\text{-}t\text{-}Bu)_3]_2(O_2C\text{-}CO_2)$, W_4(OXA). To a flask containing 1.000 g (1.30 mmol) of $W_2(O_2C\text{-}t\text{-}Bu)_4$ and 0.064 g (0.72 mmol) of oxalic acid was added 20 mL of toluene. The reaction mixture was stirred at room temperature for 4 days. The initial yellow solution turned green within minutes and then more slowly changed to a deep blue color, and finally a blue solid fell out of solution. The blue solid was isolated by filtration through a fine frit, washed with 3 × 15 mL of toluene followed by 2 × 15 mL of hexane, and then dried under vacuum to yield 0.402 g (43%) of analytically pure material: ^{1}H NMR (22 °C) pyridine-d_5 δ 1.46 (s, 36 H), 1.54 (s, 18 H); dimethyl sulfoxide-d_6 δ 1.45 (s, 18 H), 1.47 (s, 36 H); IR (cm^{-1}) 2955 (m), 1480 (s), 1465 (s), 1460 (s), 1438 (vs), 1405 (s), 1362 (ms), 1220 (s), 895 (m), 605 (m). Anal. Calcd for $C_{32}H_{54}O_{16}W_4$: C, 26.87; H, 3.81. Found: C, 27.06; H, 3.76.

$[W_2(O_2C\text{-}t\text{-}Bu)_3]_2(O_2C\text{-}1,4\text{-}C_6F_4\text{-}CO_2)$, W_4(PFT). To a flask containing 0.500 g (0.65 mmol) of $W_2(O_2C\text{-}t\text{-}Bu)_4$ and 0.095 g (0.39 mmol) of tetrafluoroterephthalic acid was added 15 mL of toluene. The reaction was stirred at room temperature for 4 days over which time the color changed from yellow to green to dark blue and a blue precipitate formed. The reaction mixture was filtered through a fine frit, and the blue solid was washed with 2 × 15 mL of toluene followed by 2 × 15 mL of hexane and then dried under vacuum to yield 0.479 g (94%) of analytically pure material: ^{1}H NMR (22 °C) acetone-d_6 δ 1.37 (s, 36 H), 1.40 (s, 18 H); ^{19}F NMR (22 °C), acetone-d_6 δ −141.14 (s); IR (cm^{-1}) 2967 (m), 1485 (vs), 1458 (s), 1440 (ms), 1412 (s), 1366 (ms), 1221 (ms), 997 (m), 895 (w), 741 (m), 615 (w). Anal. Calcd for $C_{38}H_{54}F_4O_{16}W_4$: C, 28.92; H, 3.45; F, 4.82. Found: C, 29.19; H, 3.24; F, 5.81.

$[W_2(O_2C\text{-}t\text{-}Bu)_3]_2(O_2C\text{-}1,8\text{-}C_{14}H_8\text{-}CO_2)$, W_4(AND). To a flask containing 0.300 g (0.39 mmol) of $W_2(O_2C\text{-}t\text{-}Bu)_4$ and 0.052 g (0.20 mmol) of anthracene-1,8-dicarboxylic acid was added 10 mL of toluene. The reaction turned green immediately and was stirred at room temperature for 5 days to ensure complete reaction. The green solid was isolated by filtration through a fine frit, washed with 3 × 10 mL of toluene followed by 2 × 10 mL of hexane then dried under vacuum to yield 0.215 g (69%) of analytically pure material: ^{1}H NMR (22 °C) pyridine-d_5 δ 1.47 (s, 36 H), 1.61 (s, 18 H), 7.52 (t, $^3J_{HH}$ = 9 Hz, 2 H), 7.55 (d, $^3J_{HH}$ = 9 Hz, 2 H), 8.12 (dd, $^3J_{HH}$ = 7 Hz, $^4J_{HH}$ = 2 Hz, 2 H), 8.15 (s, 1 H), 13.14 (s, 1 H); IR (cm^{-1}) 2961 (ms), 1482 (s), 1458 (vs), 1410 (s), 1360 (m), 1219 (ms), 895 (w), 610 (w). Anal. Calcd for $C_{46}H_{62}O_{16}W_4$: C, 34.39; H, 3.89. Found: C, 34.78; H, 3.65.

$[W_2(O_2C\text{-}t\text{-}Bu)_3]_2(O_2C\text{-}1,8\text{-}C_{14}H_{10}\text{-}CO_2)$, W_4(DAND). To a flask containing 0.500 g (0.65 mmol) of $W_2(O_2C\text{-}t\text{-}Bu)_4$ and 0.104 g (0.39 mmol) of 9,10-dihydroanthracene-1,8-dicarboxylic acid was added 10 mL of toluene. The reaction turned red immediately and was stirred at room temperature for 3 days during which time a red precipitate formed. Hexane (20 mL) was added to the reaction mixture, and the slurry was filtered through a fine frit. The red solid collected on the frit was washed with 2 × 10 mL of hexane and then dried under vacuum to yield 0.282 g (54%) of analytically pure material: ^{1}H NMR (22 °C) pyridine-d_5 δ 1.52 (s, 36 H), 1.60 (s, 18 H), 3.69 (s, 2 H), 6.24 (s, 2 H), 7.02 (d, $^3J_{HH}$ = 7 Hz, 2 H), 7.21 (t, $^3J_{HH}$ = 8 Hz, 2 H), 8.14 (d, $^3J_{HH}$ = 8 Hz, 2 H); IR (cm^{-1}) 2961 (m), 1482 (s), 1458 (vs), 1439 (ms), 1410 (s), 1364 (ms), 1219 (ms), 895 (w), 610 (w). Anal. Calcd for $C_{46}H_{64}O_{16}W_4$: C, 34.35; H, 4.01. Found: C, 35.88; H, 3.67.

$[W_2(O_2C\text{-}t\text{-}Bu)_3]_2(O_2C(C_5H_4)Fe(C_5H_4)CO_2)$, W_4(FDC). To a flask containing 0.0976 g (0.36 mmol) of 1,1′-ferrocenedicarboxylic acid was added a slurry of 0.500 g (0.65 mmol) of $W_2(O_2C\text{-}t\text{-}Bu)_4$ in 20 mL of toluene. Over a period of 3 days a maroon precipitate formed and was isolated by filtration through a fine frit. The solid was washed with 3 × 10 mL of toluene and dried under vacuum to yield 0.503 g (96%) of material. ^{1}H NMR (22 °C) pyridine-d_5 δ 1.50 (s, 36 H), 1.54 (s, 18 H), 4.32 (d, $^3J_{HH}$ = 2 Hz, 4 H), 5.12 (d, $^3J_{HH}$ = 3 Hz, 4 H).

$Mo_2(O_2C\text{-}t\text{-}Bu)_2(MeCN)_6(BF_4)_2$. The compound was prepared according to the method described previously for $Mo_2(O_2CMe)_2(MeCN)_6(BF_4)_2$.[13] To a slurry of 1.845 g (3.1 mmol) of $Mo_2(O_2C\text{-}t\text{-}Bu)_4$ in 20 mL of CH_2Cl_2 and 5 mL of MeCN was added Me_3OBF_4 (13.9 mmol) via a solids addition tube. Within 1 h all of the solid material had dissolved, and the solution was bright red. After 12 h the reaction mixture was concentrated and cooled to −20 °C. Overnight red crystals formed and were isolated by cannula removal of the mother liquor, washing with diethyl ether, and drying under vacuum: ^{1}H NMR (22 °C) acetonitrile-d_3 δ 1.54 (s, 18 H), 1.95 (s, 18 H); methylene chloride-d_2 δ 1.56 (s, 18 H), 1.97 (s, 6 H), 2.81 (s, 12 H).

$Mo_2(O_2C\text{-}t\text{-}Bu)_3(MeCN)_2(BF_4)$. The compound can be prepared by two methods. In the first procedure 15 mL of MeCN was added to a flask containing 0.525 g (0.88 mmol) of $Mo_2(O_2C\text{-}t\text{-}Bu)_4$ and 0.716 g (0.88 mmol) of $Mo_2(O_2C\text{-}t\text{-}Bu)_2(MeCN)_6(BF_4)_2$ and heated to 70 °C for 24 h. Removal of the volatiles under vacuum yielded a peach-colored powder that contained 80% $Mo_2(O_2C\text{-}t\text{-}Bu)_3(MeCN)_2(BF_4)$, 10% $Mo_2(O_2C\text{-}t\text{-}Bu)_4$, and 10% $Mo_2(O_2C\text{-}t\text{-}Bu)_2(MeCN)_6(BF_4)_2$ by ^{1}H NMR. The solid was treated with repeated washings with toluene to remove the $Mo_2(O_2C\text{-}t\text{-}Bu)_4$ and subsequently dried under vacuum. ^{1}H NMR of the resulting material indicated $Mo_2(O_2C\text{-}t\text{-}Bu)_2(MeCN)_6(BF_4)_2$ as the only impurity (11%).

(36) Golden, R.; Stock, L. M. *J. Am. Chem. Soc.* **1972**, *94*, 3080.
(37) Newkone, G. R.; Garbis, S. J.; Majestic, V. K.; Fronczek, F. R.; Chiari, G. *J. Org. Chem.* **1981**, *46*, 833.

In the second procedure, 5.0 mL (5.0 mmol) of a 1.0 M solution of Et_3OBF_4 in dichloromethane was added to a flask containing 3.000 g (5.0 mmol) of $Mo_2(O_2C\text{-}t\text{-}Bu)_4$ slurried in 40 mL of MeCN. The reaction was heated to 70 °C for 5 h after which time the orange solution was filtered hot, and the volatile components were removed under vacuum to yield a peach-colored powder. The product was further purified according to the above procedure to yield a material of composition $Mo_2(O_2C\text{-}t\text{-}Bu)_3(MeCN)_2(BF_4)$ as determined by ^1H NMR and elemental analysis: ^1H NMR (22 °C) acetonitrile-d_3 δ 1.34 (s, 9 H), 1.56 (s, 18 H), 1.95 (s, 6 H). Anal. Calcd for $C_{19}H_{33}BF_4N_2O_6Mo_2$: C, 34.36; H, 5.01; N, 4.22. Found: C, 34.59; H, 5.06; N, 5.61.

$[Mo_2(O_2C\text{-}t\text{-}Bu)_3]_2$(2,3-dioxyquinoxaline), Mo_4(DOQ). To a slurry containing 0.109 g (0.67 mmol) of 2,3-dihydroxyquinoxaline in 10 mL of tetrahydrofuran was added 0.81 mL (1.30 mmol) of a 1.6 M solution of *n*-butyllithium in hexane. Deprotonation was determined to be complete upon dissolution of the solid and the persistence of a light yellow color. The solution was cooled to 0 °C and then transferred dropwise via cannula to a freshly prepared solution of 0.800 g (1.28 mmol) of $Mo_2(O_2C\text{-}t\text{-}Bu)_3(MeCN)_2(BF_4)$ in 20 mL of tetrahydrofuran, also cooled to 0 °C. The reaction was stirred at 0 °C for 5 min, then allowed to warm to room temperature, and stirred for an additional 2 h. The volatiles were removed under vacuum, and the resulting residue was triturated with hexane to yield an orange-brown powder. The powder was extracted with tetrahydrofuran, filtered through Celite, and then evacuated to dryness to give 0.675 g (91%) of crude material. The material was recrystallized from a concentrated solution of dimethylformamide at −20 °C to give orange needles: ^1H NMR (22 °C) acetone-d_6 δ 1.34 (s, 36 H), 1.44 (s, 18 H), 6.01 (dd, $^3J_{HH}$ = 6 Hz, 3 Hz, 2 H), 6.96 (dd, $^3J_{HH}$ = 6 Hz, 3 Hz, 2 H); IR (cm^{-1}) 2961 (m), 1487 (vs), 1420 (s), 1379 (m), 1364 (m), 1225 (ms), 897 (w), 799 (w), 747 (w), 619 (m). Anal. Calcd for $C_{38}H_{58}N_2O_{14}Mo_4$: C, 39.67; H, 5.08. Found: C, 39.24; H, 4.74.

$[Mo_2(O_2C\text{-}t\text{-}Bu)_3]_2$(2,7-dioxynaphthyridine), Mo_4(DON). To a slurry containing 0.108 g (0.67 mmol) of 2,7-dihydroxynaphthyridine in 10 mL of methanol was added 0.30 mL (1.30 mmol) of a 4.4 M solution of sodium methoxide in methanol. The material dissolved upon deprotonation and formation of the disodium salt. The solution was cooled to 0 °C and added dropwise via cannula to a freshly prepared solution of 0.800 g (1.28 mmol) of $Mo_2(O_2C\text{-}t\text{-}Bu)_3(MeCN)_2(BF_4)$ in 20 mL of tetrahydrofuran, also cooled to 0 °C. The reaction was stirred at 0 °C for 1 h and then at room temperature for 2 h, after which time the volatile components were removed under vacuum to give an orange-brown residue. The residue was triturated with hexane and dried under vacuum to give a dry orange powder. The powder was treated with 30 mL of toluene, and the solution was filtered through Celite (to extract any residual $Mo_2(O_2C\text{-}t\text{-}Bu)_4$). The filtrate was discarded. The toluene insoluble residue was extracted with 40 mL of tetrahydrofuran, filtered through the same celite pad, and concentrated to dryness to yield 0.520 g (70%) of crude product. The material was recrystallized from concentrated tetrahydrofuran solutions at −20 °C to yield irregular shaped orange crystals: ^1H NMR (22 °C) acetone-d_6 δ 1.51 (s, 36 H), 1.62 (s, 18 H), 7.11 (d, $^3J_{HH}$ = 9 Hz, 2 H), 7.56 (d, $^3J_{HH}$ = 9 Hz, 2 H); variable-temperature ^1H NMR methylene chloride-d_2/methanol-d_4 (2:1) +25 °C δ 1.26 (s, 36 H), 1.38 (s, 18 H), 7.06 (d, $^3J_{HH}$ = 9 Hz, 2 H), 7.75 (d, $^3J_{HH}$ = 9 Hz, 2 H); −90 °C δ 1.04 (s, 18 H), 1.26 (s, 18 H), 1.26 (s, 18 H), 7.03 (d, 2 H), 7.72 (d, 2 H); $\Delta G^{\dagger}$ (−50 °C) = 10.4 kcal/mol; IR (cm^{-1}) 2963 (m), 1510 (vs), 1487 (vs), 1458 (m), 1420 (s), 1373 (ms), 1358 (m), 1225 (m), 898 (w), 615 (m). Anal. Calcd for $C_{38}H_{58}H_2O_{14}Mo_4$: C, 39.67; H, 5.08. Found: C, 39.08; H, 4.97.

$[Mo_2(O_2C\text{-}t\text{-}Bu)_3]_2(O_2C\text{-}CO_2)(BF_4)$, Mo_4(OXA)(BF_4). A solution of 0.076 g (0.28 mmol) of $(\eta^5\text{-}C_5H_5)_2FeBF_4$ in 10 mL of dichloromethane was added via cannula to a stirred solution of 0.300 g (0.28 mmol) of $[Mo_2(O_2C\text{-}t\text{-}Bu)_3]_2(O_2C\text{-}CO_2)$ in 25 mL of tetrahydrofuran. The red solution turned red-brown upon mixing and was stirred at room temperature overnight. The reaction mixture was concentrated to 5 mL after which 20 mL of hexane was added resulting in the formation of a brick-red precipitate. The solid was isolated by filtration, washed with 4 × 10 mL of hexane to extract any ferrocene, and then dried under vacuum to yield 0.195 g (60%) of material: ESR (22 °C) tetrahydrofuran g_{iso} = 1.93; IR (cm^{-1}) 2963 (m), 1543 (s), 1487 (vs), 1460 (m), 1420 (s), 1379 (m), 1364 (m), 1302 (m), 1225 (ms), 1084 (m, BF_4), 899 (w), 777 (m), 617 (m). Anal. Calcd for $C_{32}H_{54}BF_4O_{16}Mo_4$: C, 32.98; H, 4.67. Found: C, 31.13; H, 3.94.

$[Mo_2(O_2C\text{-}t\text{-}Bu)_3]_2(O_2C\text{-}1,4\text{-}C_6F_4\text{-}CO_2)(PF_6)$, Mo_4(PFT)(PF_6). A solution of 0.021 g (0.08 mmol) of $AgPF_6$ dissolved in 5 mL of tetrahydrofuran was added via cannula to a stirred solution of 0.100 g (0.08 mmol) of $[Mo_2(O_2C\text{-}t\text{-}Bu)_3]_2(O_2C\text{-}1,4\text{-}C_6F_4\text{-}CO_2)$ in 20 mL of tetrahydrofuran. Silver metal fell out of solution upon stirring for 30 min at room temperature. The Ag was removed by filtration on a fine frit. The filtrate was concentrated to dryness to yield 0.104 g of red-orange material. A satisfactory analysis of this compound could not be obtained because the material could never be isolated completely free of solvent: ESR (−196 °C) powder $g_{\parallel}$ = 1.92, $g_{\perp}$ = 1.88; IR (cm^{-1}) 2965 (m), 1541 (ms), 1487 (vs), 1420 (s), 1393 (ms), 1381 (ms), 1366 (m), 1223 (ms), 1111 (m, PF_6), 995 (m), 899 (w), 747 (m), 617 (m).

$[W_2(O_2C\text{-}t\text{-}Bu)_3]_2(O_2C\text{-}CO_2)(BF_4)$, W_4(OXA)(BF_4). A solution of 0.038 g (0.14 mmol) of $(\eta^5\text{-}C_5H_5)_2FeBF_4$ in 12 mL of dichloromethane was added via cannula to a solution of 0.200 g (0.14 mmol) of $[W_2(O_2C\text{-}t\text{-}Bu)_3]_2(O_2C\text{-}CO_2)$ in 8 mL of tetrahydrofuran. The solution turned from blue to turquoise upon mixing. The reaction was stirred for 8 h at room temperature after which time the solvents were removed under vacuum. Hexane (3 × 20 mL) was used to extract the ferrocene, and the solid remaining was dried under vacuum to give 0.208 g of product: ESR (−150 °C) powder $g_{\parallel}$ = 1.82, $g_{\perp}$ = 1.78; IR (cm^{-1}) 2971 (m), 1487 (vs), 1458 (s), 1428 (s), 1379 (m), 1366 (ms), 1223 (s), 1107 (m, BF_4), 1084 (m, BF_4), 625 (m). Anal. Calcd for $C_{32}H_{54}BF_4O_{16}W_4\cdot 1.3(C_4H_8O)$: C, 27.67; H, 4.02; F, 4.95. Found: C, 28.08; H, 3.60; F, 4.64.

$[W_2(O_2C\text{-}t\text{-}Bu)_3]_2(O_2C\text{-}1,4\text{-}C_6F_4\text{-}CO_2)(BF_4)$, W_4(PFT)(BF_4). A solution of 0.022 g (0.08 mmol) of $(\eta^5\text{-}C_5H_5)_2FeBF_4$ in 10 mL of dichloromethane was added via cannula to a stirred solution of 0.130 g (0.08 mmol) of $[W_2(O_2C\text{-}t\text{-}Bu)_3]_2(O_2C\text{-}1,4\text{-}C_6F_4\text{-}CO_2)$ in 5 mL of tetrahydrofuran. The reaction changed from blue to blue-green upon addition, and the reaction was further stirred for 24 h. The solvents were removed under vacuum, and the ferrocene was extracted with 4 × 10 mL of hexane. The resulting blue solid was dried under vacuum to yield 0.113 g of product: ESR (−196 °C), powder $g_{\parallel}$ = 2.00, $g_{\perp}$ = 1.95; IR (cm^{-1}) 2970 (m), 1487 (vs), 1458 (s), 1428 (s), 1368 (s), 1223 (s), 1107 (m, BF_4), 1084 (m, BF_4), 739 (m), 627 (m). Anal. Calcd for $C_{38}H_{54}BF_8O_{16}W_4\cdot 3.5(C_4H_8O)$: C, 32.57; H, 4.31; F, 7.93. Found: C, 33.07; H, 3.79; F, 9.14.

Computational Procedures. Molecular orbital calculations were performed on a VAX computer system with the Fenske–Hall approximate MO method.[21] All atomic wave functions used were generated by the method of Bursten, Jensen, and Fenske.[38] Contracted double-ζ representations were used for the W 5d, Mo, 4d, N 2p, O 2p, and C 2p AOs. The W 6s and 6p exponents were fixed at 2.40, and the Mo 5s and 5p exponents were fixed at 2.00 and 1.60, respectively. All calculations were converged with a self-consistent field iterative technique by using a convergence criteria of 0.0010 as the largest deviation between atomic orbital populations for successive cycles.

The interatomic distances and angles of $Mo_2(O_2C\text{-}t\text{-}Bu)_4$[39] were used to construct the atomic parameters for the M_2 cores of the model systems $[M_2(O_2CH)_3]_2(\mu\text{-}O_2CCO_2)$ (M = Mo, W) and $[W_2(O_2CH)_4]_2$. For the oxalate-bridged system a C–C distance of 1.40 Å was used, and the system was idealized to D_{2h} symmetry. The two ditungsten tetraformate units of $[W_2(O_2CH)_4]_2$ were oriented in an "offset parallel" mode such that intermolecular W–O and W–W distances of 2.665 and 3.080 Å, respectively, were attained with overall C_{2h} symmetry. The atomic coordinates of the individual $Mo_2H_8^{4-}$ units of the $[Mo_2H_8]_2^{8-}$ model system were generated with the following distances and angles: Mo–Mo = 2.14 Å, Mo–H = 1.80 Å, Mo–Mo–H = 90°. Calculations of $[Mo_2H_8]_2^{8-}$ were performed at the internuclear Mo–Mo distances of 2.40, 2.30, 2.20, and 2.14 Å under D_{4h} symmetry. The coordinates for the model complex $[Mo_2H_6]_2(\mu\text{-}O_2N_2C_8H_4]^{6-}$ were taken from the crystal structure of Mo_4(DON) with the following changes. The pivalate ligands were replaced with hydride ligands assuming the bond length Mo–H = 1.80 Å, and the Mo_4 chain was constrained to be linear (Mo–Mo–Mo = 180°, Mo–Mo = 2.40 Å) giving rise to overall C_{2v} symmetry.

Crystallographic Study. General operating procedures and listings of programs have been described.[40]

$[Mo_2(O_2C\text{-}t\text{-}Bu)_3]$(2,7-dioxynaphthyridine), Mo_4(DON). A summary of crystal data is given in Table VI. A suitable crystal was cooled to −169 °C for characterization and data collection.

A search of a limited hemisphere of reciprocal space revealed a set of diffraction maxima with no symmetry or systematic absences. Therefore there are two possible tryclinic space groups: $P1$ and $P\bar{1}$. We chose the centrosymmetric one; the successful solution of the structure verified this choice. Data were collected in the usual manner with a continuous θ–2θ scan with fixed backgrounds. Data were reduced to a unique set of intensities and associated σ's in the usual manner.

The structure was solved by the usual combination of direct methods (MULTANS78) and Fourier synthesis. All hydrogen atoms positions were calculated with idealized geometries and d(C–H) = 0.95 Å. These

(38) Bursten, B. E.; Jensen, J. R.; Fenske, R. F. *J. Chem. Phys.* **1978**, *68*, 3320.

(39) Cotton, F. A.; Extine, M.; Gage, L. D. *Inorg. Chem.* **1978**, *17*, 172.

(40) Chisholm, M. H.; Folting, K.; Huffman, J. C.; Kirkpatrick, C. C. *Inorg. Chem.* **1984**, *23*, 1021.

calculated positions were fixed for the final cycles refinement. The largest peaks of the final difference Fourier were situated close to the atoms of solvent molecules.

Acknowledgment. We thank the National Science Foundation for support. R.H.C. is a National Science Foundation Postdoctoral Fellow.

Registry No. Mo_4(OXA), 123358-63-4; W_4(OXA), 123380-77-8; Mo_4(PFT), 123358-64-5; W_4(PFT), 123358-65-6; W_4(FDC), 136301-48-9; Mo_4(DOQ), 136327-68-9; Mo_4(DAND), 123358-68-9; W_4(DAND), 123380-78-9; Mo_4(AND), 123358-66-7; W_4(AND), 123358-67-8; Mo_4(DON), 136301-49-0; Mo_4(OXA)$^+$, 136301-43-4; W_4(OXA)$^+$, 136301-45-6; Mo_4(PFT)$^+$, 136301-47-8; W_4(PFT)$^+$, 136327-67-8; $Mo_2(O_2C$-t-$Bu)_4$, 55946-68-4; $W_2(O_2C$-t-$Bu)_4$, 86728-84-9; $Mo_2(O_2C$-t-$Bu_2)(MeCN)_6(BF_4)_2$, 134078-47-0; $Mo_2(O_2C$-t-$Bu)_3(MeCN)_2(BF_4)$, 134078-49-2; $[Mo_2(O_2CH)_3]_2(\mu$-$O_2CCO_2)$, 136301-50-3; $[W_2(O_2CH)_3]_2(\mu$-$O_2CCO_2)$, 136301-51-4; $[W_2(O_2CH)_4]_2$, 136327-69-0; $[Mo_2H_6]_2(\mu$-2,7-$O_2N_2C_8H_4)^{6-}$, 136301-52-5; W, 7440-33-7; Mo, 7439-98-7; 1,1'-ferrocenedicarboxylic acid, 1293-87-4.

Supplementary Material Available: Tables of fractional coordinates and thermal parameters, anisotropic thermal parameters, and bond distances and bond angles and VERSORT drawings (11 pages); listings of F_o and F_c values (18 pages). Ordering information is given on any current masthead page.

Thermal and Photochemical Transformations of Organoiridium Phosphide Complexes. Mechanistic Studies on Carbon–Phosphorus Bond Formation To Generate Cyclometalated Hydride Complexes by α-Hydride Abstraction

Michael D. Fryzuk,*,† Kiran Joshi, Raj K. Chadha,§ and Steven J. Rettig‡

Contribution from the Department of Chemistry, University of British Columbia, 2036 Main Mall, Vancouver, BC, Canada V6T 1Z1. *Received April 23, 1991*

Abstract: The thermal and photolytic transformations of a series of methyliridium(III) phosphide complexes are described. Complexes of the formula $Ir(CH_3)PR_2[N(SiMe_2CH_2PPh_2)_2]$ (R = Ph, Me) rearrange thermally to generate the corresponding cyclometalated derivatives *fac*-$Ir(\eta^2$-$CH_2PR_2)H[N(SiMe_2CH_2PPh_2)_2]$; continued thermolysis results in the formation of the iridium(I) phosphine complexes $Ir(PMeR_2)[N(SiMe_2CH_2PPh_2)_2]$. Under photolytic conditions the phosphide derivatives rearrange directly to the phosphine complexes with no observable intermediates. The phenylphosphide complex $Ir(CH_3)PHPh[N(SiMe_2CH_2PPh_2)_2]$ rearranges directly to the phosphine derivative $Ir(PHPhMe)[N(SiMe_2CH_2PPh_2)_2]$ both thermally and photolytically with no observable intermediates. Crystals of $Ir(CH_3)PPh_2[N(SiMe_2CH_2PPh_2)_2]$ are monoclinic with a = 13.506 (3) Å, b = 13.665 (3) Å, c = 22.816 (7) Å, β = 92.35 (2)°, Z = 4, D_c = 1.454 g cm^{-3}, and space group $P2_1/c$. The structure was solved by the Patterson method and refined by full-matrix least-squares procedures to R = 0.034 and R_w = 0.037 for 3993 reflections with $I \geq 3\sigma(I)$. Crystals of *fac*-$Ir(\eta^2$-$CH_2PPh_2)H[N(SiMe_2CH_2PPh_2)_2]$ are monoclinic with a = 9.253 (2) Å, b = 21.950 (5) Å, c = 20.081 (4) Å, β = 90.74 (2)°, Z = 4, D_c = 1.50 g cm^{-3}, and space group $P2_1/c$. The structure was solved by conventional heavy-atom techniques and was refined in blocks (with the Ir atom in every cycle) by using least-squares procedures down to R = 0.0356 and R_w = 0.0370 for 4448 reflections with $I \geq 3\sigma(I)$. Mechanistic studies showed that the formation of the cyclometalated hydride does not involve reductive transfer of the methyl and the phosphide ligands to form a phosphine complex followed by intramolecular C–H bond activation, rather C–H bond abstraction occurs first followed then by C–P bond formation. Transition-state arguments are used to rationalize the difference in the reactivity of the phenylphosphide complex for which no cyclometalated intermediate was detected.

Introduction

Metal complexes mediate many complex transformations by virtue of the fact that the reacting moieties are proximate to one another (i.e., cis disposed) and under the influence of both the metal center and the ancillary ligands. The formation of C–C, C–H, and C–X bonds (X is a heteroatom, e.g., O, N, Si, P, etc.) within the coordination sphere of a metal complex is of both fundamental interest[1] and practical interest in the development of new reagents for organic synthesis.[2] Although a number of studies on the formation of C–X bonds have been made, in particular, formation of C–O[3] and C–N[4] functionalities, little has been reported on the formation of carbon–phosphorus bonds[5] (C–P) at a transition-metal center. Part of the reason for the dearth of results in this area is that there are very few metal complexes that contain both a hydrocarbyl ligand and a suitable phosphorus donor such as a phosphide (PR_2^-) to study *intramolecular* C–P bond formation.

Sometime ago, we reported[6] the preparation and some reaction studies[7] of a series of methyliridium phosphide complexes of the general formula $Ir(CH_3)PR_2[N(SiMe_2CH_2PPh_2)_2]$ (R = aryl). These complexes were subsequently shown[8] to rearrange to cy-

Scheme I

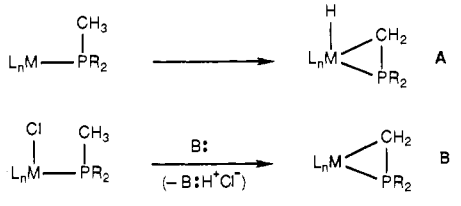

† E. W. R. Steacie Fellow (1990–92).

‡ Present address: Department of Chemistry, University of California at San Diego, La Jolla, CA 92093.

§ Professional Officer: UBC Crystallographic Service.

(1) Collman, J. P.; Hegedus, L. S.; Norton, J. R.; Finke, R. G. *Principles and Applications of Organotransition Metal Chemistry*; University Science Books: Mill Valley, CA, 1987; pp 669–937.

(2) (a) Posner, G., Ed. *Pure Appl. Chem.* **1988**, *60*, 1–144. (b) Hegedus, L. S. *J. Organomet. Chem.* **1988**, *342*, 147. (c) Parshall, G. W.; Nugent, W. A.; Chan, D. M. T.; Tam, W. *Pure Appl. Chem* **1985**, *57*, 1809. (d) Negishi, E. *Organometallics in Organic Synthesis*; Wiley: New York, NY, 1980.

(3) (a) Bernard, K. A.; Atwood, J. D. *Organometallics* **1989**, *8*, 795. (b) Komiya, S.; Akai, Y.; Tanaka, T.; Yamamoto, T.; Yamamoto, A. *Organometallics* **1985**, *4*, 1130.

(4) (a) Murahashi, S.-I.; Yoshimura, N.; Tsumiyama, T.; Kojima, T. *J. Am. Chem. Soc.* **1983**, *105*, 5002. (b) Fryzuk, M. D.; MacNeil, P. A.; Rettig, S. J. *J. Organomet. Chem.* **1987**, *332*, 345.

0002-7863/91/1513-8724$02.50/0